Chemical genetic screen identifies *Toxoplasma* DJ-1 as a regulator of parasite secretion, attachment, and invasion

Carolyn I. Hall[a], Michael L. Reese[a], Eranthie Weerapana[b], Matthew A. Child[c], Paul W. Bowyer[c], Victoria E. Albrow[c], Jeralyn D. Haraldsen[d], MacDonald R. Phillips[c], Edgar Deu Sandoval[c], Gary E. Ward[d], Benjamin F. Cravatt[b], John C. Boothroyd[a], and Matthew Bogyo[a,c,1]

Departments of [a]Microbiology and Immunology and [c]Pathology, Stanford University School of Medicine, Stanford, CA 94305; [b]Department of Chemical Physiology, The Scripps Research Institute, La Jolla, CA 92037; and [d]Department of Microbiology and Molecular Genetics, University of Vermont, Burlington, VT 05405

Edited* by James A. Wells, University of California, San Francisco, CA, and approved May 18, 2011 (received for review April 8, 2011)

***Toxoplasma gondii* is a member of the phylum Apicomplexa that includes several important human pathogens, such as *Cryptosporidium* and *Plasmodium falciparum*, the causative agent of human malaria. It is an obligate intracellular parasite that can cause severe disease in congenitally infected neonates and immunocompromised individuals. Despite the importance of attachment and invasion to the success of the parasite, little is known about the underlying mechanisms that drive these processes. Here we describe a screen to identify small molecules that block the process of host cell invasion by the *T. gondii* parasite. We identified a small molecule that specifically and irreversibly blocks parasite attachment and subsequent invasion of host cells. Using tandem orthogonal proteolysis–activity-based protein profiling, we determined that this compound covalently modifies a single cysteine residue in a poorly characterized protein homologous to the human protein DJ-1. Mutation of this key cysteine residue in the native gene sequence resulted in parasites that were resistant to inhibition of host cell attachment and invasion by the compound. Further analysis of the invasion phenotype confirmed that modification of Cys127 on TgDJ-1 resulted in a block of microneme secretion and motility, even in the presence of direct stimulators of calcium release. Together, our results suggest that TgDJ-1 plays an important role that is likely downstream of the calcium flux required for microneme secretion, parasite motility, and subsequent invasion of host cells.**

The obligate intracellular protozoan parasite, *Toxoplasma gondii*, is capable of infecting almost any nucleated cell within an exceptionally broad host range. It is an opportunistic pathogen that asymptomatically infects 10–20% of the world population and can cause severe disease in congenitally infected neonates and immunocompromised individuals, in particular HIV patients (1). Although *Toxoplasma* rarely causes acute infection in healthy individuals, reactivation of latent infections can lead to toxoplasmic encephalitis, the pathology of which is associated with the parasite-mediated lytic destruction of infected host cells (2). Propagation of an infection by *Toxoplasma gondii* is dependent on the ability of the parasite to invade host cells. Although it is clear that this process requires the timed release of specific secretory organelles termed *micronemes* and *rhoptries*, relatively little is known about specific regulators of the invasion process. Because of the haploid nature of the *Toxoplasma* genome, classic forward genetic screens have proven difficult (reviewed in ref. 3). In addition, gene knockouts can result in up-regulation of related proteins or signaling pathways that can make it difficult to interpret the true function of gene products using this technology.

The use of pharmacological compounds in pathogens to perturb protein function is a viable alternative to classic genetic methods (4–8). In addition to identifying new tools for studying mechanisms of parasite invasion, small molecule screens can identify new drug targets and lead compounds for downstream development of chemotherapies. Recently a high-throughput screening effort was undertaken to identify novel inhibitors of *Toxoplasma* invasion (5). Using a large library of unbiased, small molecules in a microscopy-based invasion assay, this screen identified a number of novel molecules that can be used to dissect the complex process of host cell invasion. However, the resulting hits from the screen provided no clues as to the identity of the target protein or proteins responsible for their inhibitory activity. Although long-term follow-up efforts have identified interesting mechanisms of actions of at least one hit (9), the identification of the direct target of this compound has remained elusive. To overcome some of the issues with unbiased screening, we assembled a highly focused library of small molecules that covalently modify their targets by way of reactive electrophilic traps on the compunds (described in ref. 4). The covalent nature of the compounds greatly facilitates downstream target identification. We recently used this library to successfully identify two mechanistically distinct proteases of *Plasmodium falciparum* that cooperatively regulate erythrocyte rupture and release of newly invasive merozoites (4).

Here we report the screening of the same library of covalent inhibitors and the subsequent identification of a compound, WRR-086, that blocks *T. gondii* attachment and invasion of host cells. By converting the lead compound to a suitably labeled analog and using tandem orthogonal proteolysis–activity-based protein profiling [TOP-ABPP (10)] we identified a single cysteine residue on a poorly characterized protein, *T. gondii* DJ-1 (TgDJ-1), that is modified by WRR-086. Using parasite genetics we were able to show that mutation of this critical cysteine residue resulted in parasites that were resistant to the effects of WRR-086, suggesting that TgDJ-1 is the primary target responsible for the phenotypic effects of the compound. Further functional studies using WRR-086 indicated that disruption of TgDJ-1 function results in a block of microneme secretion and parasite motility, even in the presence of specific agents that directly induce calcium release in the parasite. Therefore, our results identify TgDJ-1 as a unique regulator of microneme secretion and motility, and suggest that this protein is downstream

Author contributions: C.I.H., M.L.R., E.W., M.A.C., P.W.B., J.D.H., G.E.W., B.F.C., and M.B. designed research; C.I.H., M.L.R., E.W., M.A.C., P.W.B., V.E.A., J.D.H., and E.D.S. performed research; C.I.H., M.L.R., E.W., M.A.C., P.W.B., V.E.A., J.D.H., M.R.P., E.D.S., G.E.W., B.F.C., J.C.B., and M.B. analyzed data; and C.I.H. and M.B. wrote the paper.

The authors declare no conflict of interest.

*This Direct Submission article had a prearranged editor.

Freely available online through the PNAS open access option.

[1]To whom correspondence should be addressed. E-mail: mbogyo@stanford.edu.

This article contains supporting information online at www.pnas.org/lookup/suppl/doi:10.1073/pnas.1105622108/-/DCSupplemental.

of calcium signaling in the cascade of molecular events that lead to the invasion of host cells.

Results

Identification of Small Molecules That Block Host Cell Invasion. We recently described the assembly of a highly directed library of 1,222 small molecule inhibitors designed to covalently modify proteases in an activity-dependent manner (library described in ref. 4). The library includes compounds that were originally designed to target a variety of cysteine and serine proteases, as well as compounds that can act as general electrophiles for enzyme targets. The covalent binding nature of this library greatly facilitates downstream target identification (described in ref. 4). We screened the library using a previously described dual-fluorescence microscopy-based assay that allows direct monitoring of parasite attachment and entry into host cells (Fig. 1*A*) (5). Compounds that showed a gross qualitative change in either the number of intracellular parasites or in the overall number of parasites per field in two out of three assays were chosen as initial hits for further analysis (Fig. 1*B*). We identified compounds that block as well as enhance parasite invasion. However, for this study we focused on compounds that inhibited parasite attachment (decrease in number of parasites per field) or invasion (decrease in number of intracellular parasites). The initial inhibitor hits were further triaged using a series of secondary assays that included overall compound purity, general toxicity to host cells/parasites, and reversibility of the inhibitory phenotype (Fig. 1*C*). At the end of this process, only five compounds were sufficiently nontoxic, showed irreversible inhibitory effects on host cell invasion, and had no gross qualitative effect when used to pretreat host cells independent of parasites (Table 1). Further quantification of the inhibitory activities of these five compounds revealed that JCP-241 and WRR-086 had similar phenotypic profiles for both attachment and invasion. We chose

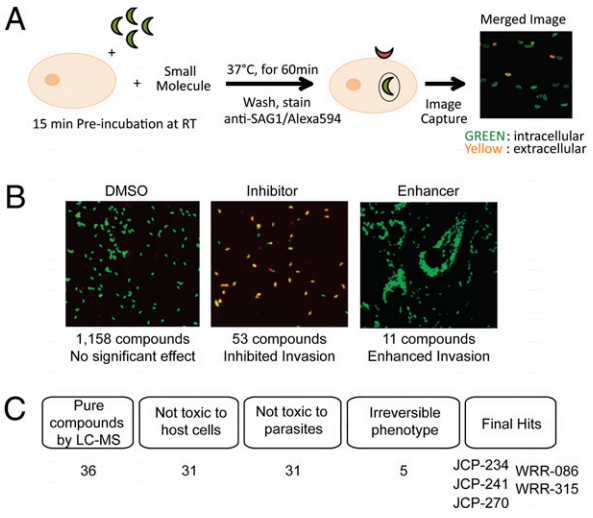

Fig. 1. Small molecule screen to identify compounds that alter host cell attachment and invasion by *T. gondii*. (*A*) Diagram of the screen in which YFP-expressing parasites were pretreated with compounds, then allowed to invade host cells, followed by antibody staining of the SAG1 surface protein on parasites that remained outside host cells. Invaded parasites are green (YFP positive), whereas those that failed to invade are yellow (YFP positive/Alexa 594 positive). RT = room temperature. (*B*) Representative fluorescent images from the dual-fluorescence screen showing vehicle (DMSO), a compound that inhibited invasion, and a compound that enhanced invasion. Total numbers of compounds screened as well as inhibitors/enhancers identified are indicated. (*C*) Triage of preliminary hits based on compound purity by LC-MS, overall toxicity to host cells (24-h compound treatment) or parasites (1-h compound treatment of extracellular parasites), and reversibility of the phenotype. The final five hits are listed.

Table 1. Phenotype summary for compounds that inhibit host cell invasion by *T. gondii*

Compound ID	Compound structure	Invasion efficiency (%)*	Attachment efficiency (%)†
JCP-234	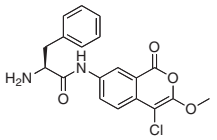	53.4	48.3
JCP-241	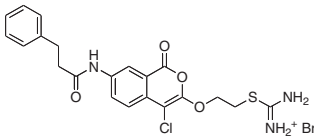	16.5	7.0
JCP-270	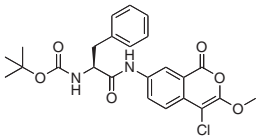	57	32.7
WRR-086	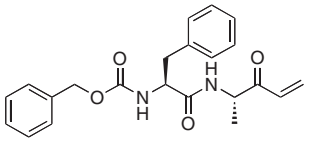	16.5	1.0
WRR-315	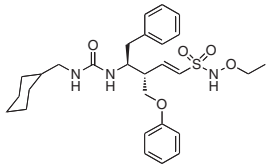	47.2	16.9

*Invasion efficiency is defined as the percentage of total parasites invaded relative to vehicle-treated controls.
†Attachment efficiency was determined by counting the average number of total parasites per field over 10 randomly selected fields and is expressed as percentage relative to vehicle-treated controls.

to focus our efforts on WRR-086, because this compound could be more readily synthesized in tagged form and contained a clear electrophile that was likely to form covalent bonds with cysteine residues.

As a first step in characterization of the phenotypic effects of WRR-086, we measured the effector concentration for half-maximum response (EC_{50}) of this compound in the attachment and invasion assay (Fig. 2*A*). These results confirmed that WRR-086 was maximally active in the low micromolar concentration range (EC_{50} = 1.9 ± 1.2 μM for attachment and EC_{50} = 5.7 ± 1.5 μM for invasion). To generate a negative control compound and determine whether the α.β-unsaturated ketone was responsible for the observed activity, we synthesized WRR-086-Ctrl, in which we reduced the double bond of the primary electrophile (Fig. 2*B*). The synthesis of this control as well as other analogs of WRR-086 was accomplished using a solid phase synthesis scheme that we developed (Fig. S1). As expected, WRR-086-Ctrl showed no inhibitory effects on either parasite attachment

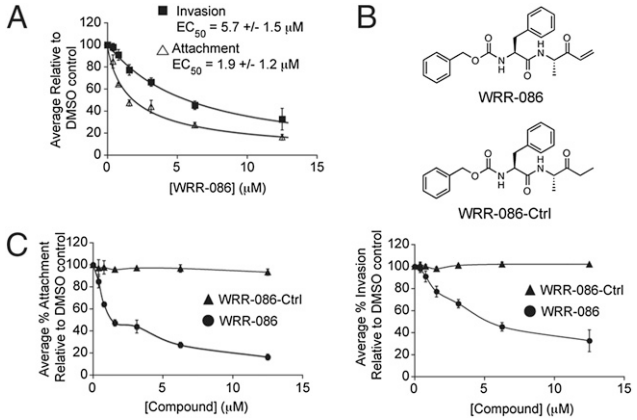

Fig. 2. WRR-086 inhibits host cell attachment and invasion. (*A*) Structures of WRR-086 and the control analog WRR-086-Ctrl. (*B*) Dose–response of WRR-086 using an Endo-synchronized attachment/invasion assay. The average percentage of attached parasites relative to DMSO-treated control parasites and average percentage of invaded parasites relative to DMSO-treated control parasites is plotted relative to concentration of WRR-086. The EC_{50} of WRR-086 in attachment to and invasion of host cells as calculated from the curve fits is shown. (*C*) Dose–response of WRR-086 and WRR-086-Ctrl compound in attachment (*Left*) and invasion (*Right*) using the Endo-synchronized attachment/invasion assay described above.

(Fig. 2*C*) or invasion (Fig. 2*D*), suggesting that the α.β-unsaturated ketone is required to react with the protein target(s).

To rule out the possibility that WRR-086 is a general inhibitor of the parasite lytic cycle we assayed overall inhibitory effects on intracellular growth using a FACS-based growth assay (Fig. S2). Parasite-infected host cells were treated with WRR-086 or vehicle control for 24 h, and then total parasite numbers per host cell were assayed by FACS. WRR-086 did not cause a significant decrease in the number of parasites per host cell at the concentrations at which we observe specific phenotypic affects on host cell invasion.

Identification of the Target of WRR-086 by TOP-ABPP. To biochemically isolate and identify the target(s) of WRR-086, we used a recently described chemoproteomic method, TOP-ABPP (10). This allowed us to label target proteins in their native environment with an alkyne analog of WRR-086 (Alkyne-086; Fig. 3*A*) and then isolate them by click chemistry conjugation to an azide-biotin affinity tag containing a tobacco etch virus (TEV) protease cleavable linker. Probe-labeled proteins were isolated by affinity purification on streptavidin beads followed by on-bead trypsin digestion to release peptides for analysis by tandem LC-MS/MS. This process leaves any probe-modified peptides attached to the streptavidin beads. These peptides were then selectively released by the addition of the TEV protease, and the sites of probe modification were determined.

We ranked proteins that were identified in the trypsin digest in two out of three replicate runs according to the total number of spectral counts identified for each protein and average fold change between vehicle and WRR-086 pretreated samples. We eliminated proteins identified in two out of three runs that had less than an average of five spectral counts combined between both runs (a complete list of proteins meeting this cutoff can be found in Table S1). We also eliminated proteins that showed less than an average 1.6-fold change between vehicle and WRR-086 pretreated samples. Finally, we cross-referenced the remaining candidates with the list of proteins identified as having specific probe-modified peptides that appeared with three or more spectral counts (a complete list of probe-modified peptides can be found in Table S2). This narrowed down our hit list to six proteins (Table 2). Among the top six candidate proteins, most were not expected to play a specific role in host cell attachment or invasion on the basis of their documented biochemical activities (*SI Discussion*). In contrast, the second protein on our list of candidate targets, annotated as "intracellular protease" (TGME49_014290), was largely uncharacterized with respect to biochemical function. Sequence alignment revealed that this protein is a homolog of *Escherichia coli* YajL and human DJ-1 (hDJ-1), which is a member of the large multifunctional DJ-1 superfamily (Fig. 3*B*). We therefore refer to the *T. gondii* protein as TgDJ-1 going forward. We could also model the structure of the dimeric protein on the basis of the solved structure of *E. coli* YajL protein (Fig. 3*C*). This model confirms that the cysteine at position 127 (Fig. 3*B*; *Toxoplasma* numbering based on start at second methionine, Met71) that is modified by WRR-086 is in close proximity to the highly conserved Cys104 of the papain protease fold.

Genetic Validation of TgDJ-1 as the Relevant Target of WRR-086. To further validate TgDJ-1 as the functionally relevant target of WRR-086 we expressed and purified the recombinant protein containing mutations according to our TOP-ABPP data. We recombinantly expressed both the WT and the C127A mutant TgDJ-1 proteins. Furthermore, because the DJ-1 protein has a highly conserved cysteine at position 104 (position 106 in the human protein) that is thought to be essential for function (11–13), we also generated the C104A mutant. Labeling of the purified proteins with a biotin-labeled version of WRR-086 indicated that the probe was able to efficiently label both the WT and the C104A mutant proteins but not the C127A mutant (Fig. 4*A*). This result confirmed that our compound is specifically reactive toward

Fig. 3. Identification of TgDJ-1 as the target of WRR-086. (*A*) Structure of Alkyne-086 for use in "click" chemistry applications. Alkyne-086 was synthesized as shown in Fig. S1. (*B*) Alignment of DJ-1 sequences from *Toxoplasma* (Tg), *Neospora* (Nc), *Plasmodium* (Pf), *Cryptosporidium* (Ch), Human (Hs), and *E. coli* YajL. Gene model in ToxoDB predicts a start codon 213 bp upstream from the beginning of the DJ-1 domain, which also contains a potential start Met. We used the downstream AUG to create the sequence shown. Arrowhead points to Cys127 that is modified by WRR-086. (*C*) Structural modeling of TgDJ-1 using structures of the dimeric *E. coli* YajL protein (Protein Data Bank ID: 2AB0). The highly conserved cysteine C104 and the Alkyne-086 binding residue C127 are indicated.

Table 2. WRR-086–modified peptides identified by TOP-ABPP

Gene ID	Protein	Molecular mass (kDa)	Modified peptide	Spectral count
TGME49_110640	Uridine phosphorylase, putative	33	K.KGDLASLIVTVGC*EQE.A	361
TGME49_014290	Intracellular protease, putative	28	K.AVAYPC*FMDQFPADMR.G	26
TGME49_090670	Cytosol aminopeptidase	60	K.TVAVVLPTC*QK.V	20
TGME49_029000	Kelch motif domain-containing protein	68	K.LAPVC*TTFSVLDVR.R	8
TGME49_089690	Glyceraldehyde-3-phosphate dehydrogenase	37	K.GIISYTDEEVVSSDFVHC*K.F	6
TGME49_047600	Conserved hypothetical protein	73	R.AVTALLDLQNFGSC*ASTAGEELVK.T	3

Modified cysteine residues are indicated by an asterisk (*).

Cys127, even in the presence of the additional five cysteines in the protein (Fig. S3).

We then generated parasites that express mutant TgDJ-1 proteins in place of the WT sequence. We replaced the endogenous, WT copy of TgDJ-1 with either a C127S (DJ1-C127S) or C127A (DJ1-C127A) mutation fused to the 3′ UTR of *GRA2*. We chose to also generate the more conservative serine mutation in case the Ala mutant perturbed the structure in vivo. Finally, we generated a control parasite line in which we replaced the endogenous copy of TgDJ-1 with a WT copy of the gene (DJ-1-WT) flanked by the 3′ UTR from *GRA2*. Correct integration of all constructs were verified by PCR and sequencing of the locus. In addition, we confirmed that the parasites expressing mutant DJ-1 sequences showed equivalent rates of attachment and invasion as the parent strain, suggesting that these mutations did not have any unexpected effects on DJ-1 function (Table S3).

We analyzed the ability of the genetically modified parasites to attach to and invade host cells in the presence of WRR-086 (Fig. 4 *B* and *C*). As expected, the original parasite line and parasites containing a copy of the WT TgDJ-1 sequence showed the expected sensitivity to WRR-086 for both attachment and invasion. Interestingly, parasites expressing the DJ1-C127S mutant only showed reduced sensitivity to the inhibitory effects of WRR-086. This finding is consistent with the reported reduced activity of the WRR-086 electrophile toward serine residues relative to cysteine (14). The DJ1-C127A mutant lacking a reactive nucleophile at position 127 was completely resistant to the attachment and invasion effects of WRR-086 at all of the concentrations tested. These results are in agreement with our initial biochemical findings and confirm that the effects of the WRR-086 on parasite attachment and invasion are mediated by its modification of Cys127 of TgDJ-1.

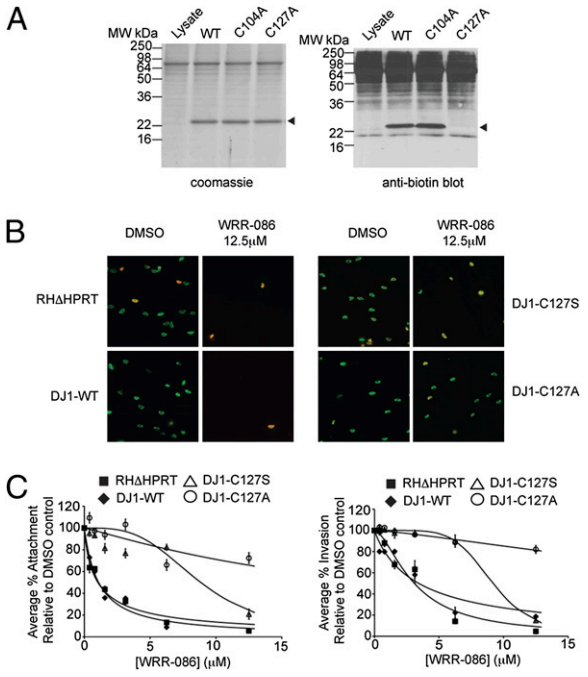

Fig. 4. Validation of TgDJ-1 as the functionally relevant target of WRR-086. (*A*) Labeling of recombinantly expressed WT, C106A, and C127A TgDJ-1 proteins. Proteins were added to total cytosolic extracts from WT (RHΔHPRT) parasites and labeled with WRR-086-biotin. Protein loading was visualized by Coomassie staining (*Left*), followed by blotting using HRP-streptavidin (*Right*). (*B*) Representative images from the dual fluorescence Endo-synchronized invasion assays showing effects at the highest dose of WRR-086 tested. Extracellular parasites are dual-stained with a mouse anti-SAG1 antibody (without permeabilization) and a rabbit anti-SAG1 antibody (with permeabilization) and appear yellow, and intracellular parasites appear green. (*C*) Dose–response of WRR-086 against host cell attachment (*Left*) and invasion (*Right*) of WT (RHΔHPRT) parasites, DJ1-WT, DJ1-C127S, and DJ1-C127A mutants. Assays were performed as described in Fig. 2. The data represent mean values ± SEMs of three independent experiments and are expressed as percentages of solvent-treated controls.

TgDJ-1 Has Diffuse Cytosolic Localization. Interestingly, the native TgDJ-1 sequence contains an upstream start codon that, if used, could result in the generation of the TgDJ-1 protein with a signal sequence. However, this upstream start site is not conserved in other highly related species, such as *Neospora*, and the consensus sequence is also not optimal. Furthermore, we identified an N-terminal methionine in our MS analysis of the protein, suggesting that the protein is not synthesized as a secretory protein with a signal sequence. However, a signal sequence could direct TgDJ-1 into the secretory transport system and into direct contact with the micronemes, a potential site of action for TgDJ-1. To address this, we generated a parasite line in which we replaced the WT copy of the gene with the WT sequence in frame with a C-terminal HA tag. These parasites behaved similarly to WT parasites and importantly, showed the same sensitivity to WRR-086 in the invasion and secretion assays (Fig. S4 *A–D*). We then performed localization studies on both extracellular and intracellular tachyzoites using an anti-HA antibody (Fig. S4*E*). The results confirm that, as observed for homologs of DJ-1 in fungi and metazoa, TgDJ-1 shows a diffuse localization consistent with a general cytosolic disposition. This localization of the protein is consistent with TgDJ-1 not being targeted to the secretory pathway in any significant quantity.

TgDJ-1 Regulates Microneme Secretion and Parasite Motility. Parasite attachment to host cells is mediated by the coordinated release of microneme proteins onto the parasite surface (15). Microneme proteins are secreted constitutively at low levels, and secretion is dramatically up-regulated (induced) upon initial attachment to host cells. This up-regulation can be induced in vitro by the treatment of extracellular parasites with calcium ionophores (15, 16) or ethanol (17), which causes an increase in intracellular parasite calcium levels and subsequent release of microneme proteins. To gain insight into the mechanism by which TgDJ-1 functions, we measured the effects of WRR-086 on both constitutive secretion and calcium-mediated induced secretion. WRR-086, but not WRR-086-Ctrl, caused a dose-dependent inhibition of secretion of the microneme resident protein, MIC2,

into the culture supernatant (EC_{50} for constitutive secretion = 5.2 ± 3.4 μM; EC_{50} for induced secretion = 6.0 ± 1.1 μM; Fig. S5). More importantly, the C127S mutant parasites were partially resistant to both induced and constitutive secretion, and the C127A mutant parasites were completely resistant to effect of WRR-086 on microneme secretion (Fig. 5). Thus, even when calcium release is directly enhanced by ethanol treatment, WRR-086 modification of TgDJ-1 blocks secretion, suggesting that it acts downstream of calcium signaling.

Secretion of microneme proteins is intimately coupled to parasite gliding motility (18). Parasites leave characteristic trails of highly abundant surface proteins and lipids while gliding. Therefore, overall gliding activity can be measured by visualizing trails produced as extracellular tachyzoites travel over coverslips coated with FBS. Treatment of parasites with WRR-086, but not WRR-086-Ctrl, leads to a dose-dependent reduction in the total number of trails observed (Fig. S6). Importantly, the concentrations of WRR-086 that induced inhibitory effects on motility closely matched the concentrations required for inhibition of invasion and microneme secretion.

Discussion

Despite the importance of attachment and invasion to the propagation of *T. gondii*, relatively little is known about the mechanisms and signaling pathways that drive these processes. There have been a few recent examples of studies that have identified both proteins (19) and natural small molecules (20) that, like TgDJ-1, regulate the process of microneme secretion. Here, using a dual-fluorescence microscopy-based assay, we identified WRR-086, a compound that inhibits parasite attachment and invasion of host cells. We were further able to show that WRR-086 modifies the parasite protein TgDJ-1 at a single cysteine residue (C127) and that it is this modification that mediates the effects of WRR-086. Finally, we show that TgDJ-1 has a general cytosolic localization and likely acts downstream of the calcium signaling that is required to initiate microneme secretion, parasite motility, and invasion of the host cell.

Although our data clearly identify TgDJ-1 as a regulator of parasite attachment and invasion, the overall lack of understanding of the function of this protein in higher eukaryotes provides no clues as to the possible mechanistic roles in this process. All of the DJ-1 homologs including TgDJ-1 have a papain-like protease domain (hence the original designation as an intracellular protease in ToxoDB), although the potential proteolytic activity of this domain remains in question. The DJ-1 proteins of higher eukaryotes have lost this enzymatic activity and are likely to have evolved a different function (21). TgDJ-1 contains the predicted active site glutamic acid (E14) and cysteine (C104) but lacks the predicted catalytic histidine. Therefore, it is highly unlikely that TgDJ-1 possesses proteolytic activity. TgDJ-1 has eight cysteines, yet we only detected modification of Cys127, indicating that this residue is specifically reactive toward the probe. Interestingly, *Plasmodium spp*. have a highly homologus DJ-1 sequence, but the cysteine at position 127 is replaced by a serine. Because serine can also act as a nucelophile, this site may also be subject to targeting with small molecule probes. Molecular modeling of TgDJ-1 using the *Pyrococcus horikoshii* PH1704 protein (Fig. S3) suggests that Cys127 is not likely to be involved in disulfide bonds and may therefore play a role in protein function. The human DJ-1 protein (hDJ-1) has only three cysteines (12). Mutational analysis of the three cysteines in hDJ-1 revealed specific functions for each, including sensing of oxidative stress (C106, human numbering), S-nitrosylation (C46 and C53), and dimerization (C46), which are critical for proper function of this protein (11–13). The only cysteine residue conserved between hDJ-1 and TgDJ-1 is the redox sensitive C106 (C104 in TgDJ-1), and we show here that this residue is not directly involved in binding WRR-086. Using the modeled structure of TgDJ-1, we determined the location of Cys127 relative to the predicted redox sensitive Cys104 (Fig. 3*C*). The overall close proximity of these residues suggest that, if in fact the conserved Cys104 is required for function, WRR-086 could act by sterically blocking substrate/ligand binding or by changing the redox environment around this residue. Unfortunately, without any known interacting proteins, it will be difficult to test this hypothesis.

To further add to the complexity of DJ-1 function, mutations in the human protein have been linked to autosomal recessive, early-onset Parkinson's disease, possibly as a result of a loss of response to oxidative stress (22, 23). Further support for the proposed role of DJ-1 in the regulation of oxidative stress in higher eukaryotes comes from evidence that it interacts with the Nrf2 transcription factor, which itself is a master regulator of the oxidative stress response (24). Furthermore other molecules, such as the calcium-dependent protein kinases (19) and abscisic acid (20), participate in host cell invasion pathways and are also central players in stress responses in plants. Indeed, it has been hypothesized that egress from the host cell is the largest stress in the life cycle of *Toxoplasma* and other intracellular pathogens, and activation of stress responses involved in invasion has been shown to be critical for *Toxoplasma* extracellular viability (25). Therefore, if the function of a stress response protein such as DJ-1 is compromised, parasites may not be able to efficiently attach and invade into the host cell. Although this is an in-

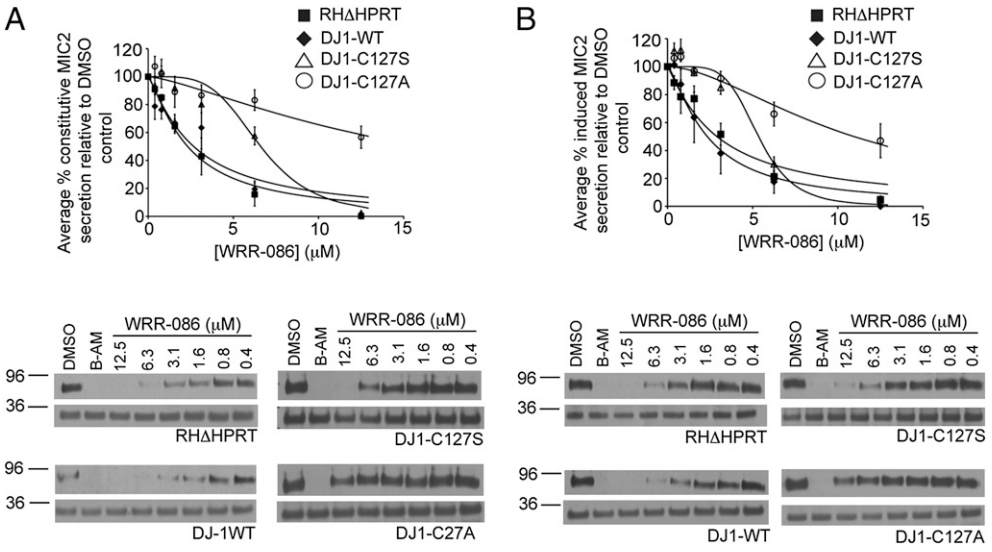

Fig. 5. DJ1-C127A parasites are resistant to the effects of WRR-086 on constitutive and ethanol-induced microneme secretion. Dose–response of RHΔHPRT, DJ1-WT, DJ1-C127S, and DJ1-C127A parasites to WRR-086 in both constitutive (*A*) and ethanol-induced (*B*) microneme secretion. Assays were performed as described in Fig. 2. The data represent mean values ± SEMs of three independent experiments and are expressed as percentages of solvent-treated controls. Representative Western blots for MIC2 (*Upper*, each pair) and the loading control SAG1 (*Lower*, each pair) are shown below the graphs.

teresting hypothesis to consider, the lack of any real mechanistic insight into DJ-1 function, despite more than a decade of rigorous study, suggests that confirmation of this hypothesis is likely to take significant additional efforts. Regardless, our results clearly show that some aspect of TgDJ-1 function is critical for the productive invasion of host cells. This, coupled with the fact that small molecules can alter its function and it is found in all *Plasmodium sp*. and many other pathogens, suggests that DJ-1 may be a previously unappreciated regulator of multiple important human infections.

Materials and Methods

Reagents and Antibodies. All chemicals and resins used for synthesis of WRR-086 and associated analogs were purchased from commercial suppliers and used without further purification. BAPTA-AM [1,2-bis-(*o*-Aminophenoxy)-ethane-N,N,N′,N′-tetraacetic acid, tetraacetoxymethyl ester] was purchased from Molecular Probes. Ethanol was purchased from Sigma and was of reagent grade or better. Vectashield fluorescence mounting medium was purchased from Vector Labs. mAb 6D10 (MIC2) has been previously described (26) (kind gift from Vern Carruthers, University of Michigan, Ann Arbor, MI). mAb 11-132 (SAG1) was purchased from Argene. mAbDG52 (SAG1) and polyclonal rabbit anti-SAG1 antibodies were both kind gifts from John Boothroyd, Stanford University School of Medicine, Stanford, CA). Alexa 488-conjugated goat anti-rabbit and Alexa 594-conjugated goat anti-mouse secondary antibodies were purchased from Molecular Probes. ECL HRP-conjugated goat anti-mouse secondary antibody was purchased from Amersham, and the KPL HRP-conjugated goat anti-mouse secondary antibody was purchased from KPL.

Parasite and Host Cell Maintenance. African Green Monkey renal epithelial cells (BS-C-1; CCL 26, American Type Culture Collection) were used as host cells for the high-throughput invasion screen. Parasites were maintained by serial passage in human foreskin fibroblasts (HFF; kind gift from John Boothroyd, Stanford University School of Medicine, Stanford, CA) cultured in DMEM (Invitrogen) supplemented with 10% FBS, 2 mM L-glutamine, and 100 μg penicillin/100 μg streptomycin per milliliter maintained at 37 °C and 5% CO_2. Parasites were harvested for use in assays by either syringe lysis of infected HFF monolayers or collection of parasites from culture supernatant after spontaneous lysis of the monolayer. Parasites were then centrifuged at 1,200 × *g* for 6 min and resuspended in HBSS (Invitrogen) supplemented with 10 mM Hepes, pH 7.0, and 1% (vol/vol) dialyzed FBS (Invitrogen) and filtered through 5-μm Millipore Syringe Filters.

Parasite Strains. TgDJ-1 constructs were amplified from genomic *Toxoplasma* RH-strain DNA. All PCR was conducted using Phusion polymerase unless otherwise noted (NEB). To create the construct for endogenous tagging and allele replacement of TgDJ-1, the 5′ targeting sequence for TgDJ1 (including the coding sequence) was initially cloned into TOPO-blunt (Invitrogen) using the forward primer 5′- GCGCGGTACCGCAGTCAAAGTGCTTGTTCCCGTC-3′ and the reverse primer 5′-gcgcgatatc tcattatcaGTACGCGTAAAGGAGCTGTGCCG-3′ (in frame with three stop codons, in lowercase). The TOPO-TgDJ1 construct was used as a template to mutate C127S or C127A according to the quick change protocol using the primers 5′-CGGTTGCGTATCCAAGCTTCATGGACCA-3′ or 5′-CGGTTGCGTATCCCGCCTTCATGGACCA-3′, and their reverse complements, respectively. The WT or mutant 5′ targeting and the TgDJ1 3′ targeting sequences were then subcloned (using the same primers) into a vector such that they flank an HPRT cassette. Transgenic parasite strains were made by electroporating the RH-strain of *T. gondii* deleted for hypoxanthine-xanthine-guanine phosphoribosyl transferase [RH(ΔHPRT)] parasites with 15 μg of linearized plasmid encoding the construct of interest and selecting for HPRT-positive parasites, as previously described (27). Clonal parasites were grown from populations by limiting dilution. Integration was verified by PCR with a primer to the GRA2 3′ UTR of the vector (5′-TGGAACTACGGTGTTTGTTCCTTTCTGCG-3′) and a primer to genomic sequence upstream to the TgDJ-1 start (and therefore to sequence not included in the targeting sequence; 5′-GAAGTTCCTGTTCTAAGGGTGATCG-3′).

High-Throughput Invasion Assay. The assembly of the directed protease inhibitor library was previously reported (4). The library was screened for compounds that block parasite invasion using a previously described high-throughput dual-fluorescence microscopy-based assay (5).

Details of the screening method as well as compound synthesis, target identification by TOP-ABPP, and secondary parasite assays are outlined in *SI Materials and Methods*.

ACKNOWLEDGMENTS. We thank William Roush and James Powers for providing some of the irreversible inhibitors of cysteine and serine proteases making up our directed library; S. Verhelst for help and advice in designing the solid-phase synthetic strategy for WRR-086 and related analogs; A. Guzzetta for HR-MS analysis of WRR-086; and Vern Carruthers for providing antibodies, reagents, and advice on performing microneme secretion and motility assays. This work was funded by a Burroughs Wellcome Trust New Investigators in Pathogenesis Award (to M.B.) and by National Institutes of Health Grants R01-AI078947 and EB005011 (to M.B.), RO1 AI21423 (to J.C.B.), R01 AI054961 (to G.E.W.). C.I.H. was supported by an American Society for Microbiology Robert D. Watksins Fellowship. M.L.R. was supported, in part, by a fellowship from the American Cancer Society.

1. Montoya JG, Liesenfeld O (2004) *Toxoplasmosis. Lancet* 363:1965–1976.
2. Luft BJ, Remington JS (1992) Toxoplasmic encephalitis in AIDS. *Clin Infect Dis* 15: 211–222.
3. Mital J, Ward GE (2008) Current and emerging approaches to studying invasion in apicomplexan parasites. *Subcell Biochem* 47:1–32.
4. Arastu-Kapur S, et al. (2008) Identification of proteases that regulate erythrocyte rupture by the malaria parasite *Plasmodium falciparum*. *Nat Chem Biol* 4:203–213.
5. Carey KL, Westwood NJ, Mitchison TJ, Ward GE (2004) A small-molecule approach to studying invasive mechanisms of *Toxoplasma gondii*. *Proc Natl Acad Sci USA* 101: 7433–7438.
6. Greenbaum DC, et al. (2002) A role for the protease falcipain 1 in host cell invasion by the human malaria parasite. *Science* 298:2002–2006.
7. Phillips CI, Bogyo M (2005) Proteomics meets microbiology: Technical advances in the global mapping of protein expression and function. *Cell Microbiol* 7:1061–1076.
8. Puri AW, Bogyo M (2009) Using small molecules to dissect mechanisms of microbial pathogenesis. *ACS Chem Biol* 4:603–616.
9. Heaslip AT, et al. (2010) A small-molecule inhibitor of *T. gondii* motility induces the posttranslational modification of myosin light chain-1 and inhibits myosin motor activity. *PLoS Pathog* 6:e1000720.
10. Weerapana E, Speers AE, Cravatt BF (2007) Tandem orthogonal proteolysis-activity-based protein profiling (TOP-ABPP)—a general method for mapping sites of probe modification in proteomes. *Nat Protoc* 2:1414–1425.
11. Anderson PC, Daggett V (2008) Molecular basis for the structural instability of human DJ-1 induced by the L166P mutation associated with Parkinson's disease. *Biochemistry* 47:9380–9393.
12. Ito G, Ariga H, Nakagawa Y, Iwatsubo T (2006) Roles of distinct cysteine residues in S-nitrosylation and dimerization of DJ-1. *Biochem Biophys Res Commun* 339:667–672.
13. Moore DJ, Zhang L, Dawson TM, Dawson VL (2003) A missense mutation (L166P) in DJ-1, linked to familial Parkinson's disease, confers reduced protein stability and impairs homo-oligomerization. *J Neurochem* 87:1558–1567.
14. Weerapana E, Simon GM, Cravatt BF (2008) Disparate proteome reactivity profiles of carbon electrophiles. *Nat Chem Biol* 4:405–407.
15. Carruthers VB, Giddings OK, Sibley LD (1999) Secretion of micronemal proteins is associated with toxoplasma invasion of host cells. *Cell Microbiol* 1:225–235.
16. Arrizabalaga G, Boothroyd JC (2004) Role of calcium during *Toxoplasma gondii* invasion and egress. *Int J Parasitol* 34:361–368.
17. Carruthers VB, Moreno SN, Sibley LD (1999) Ethanol and acetaldehyde elevate intracellular [Ca2+] and stimulate microneme discharge in *Toxoplasma gondii*. *Biochem J* 342:379–386.
18. Wetzel DM, Chen LA, Ruiz FA, Moreno SN, Sibley LD (2004) Calcium-mediated protein secretion potentiates motility in *Toxoplasma gondii*. *J Cell Sci* 117:5739–5748.
19. Billker O, Lourido S, Sibley LD (2009) Calcium-dependent signaling and kinases in apicomplexan parasites. *Cell Host Microbe* 5:612–622.
20. Nagamune K, Moreno SN, Chini EN, Sibley LD (2008) Calcium regulation and signaling in apicomplexan parasites. *Subcell Biochem* 47:70–81.
21. Bandyopadhyay S, Cookson MR (2004) Evolutionary and functional relationships within the DJ1 superfamily. *BMC Evol Biol* 4:6.
22. Bonifati V, et al. (2003) DJ-1(PARK7), a novel gene for autosomal recessive, early onset parkinsonism. *Neurol Sci* 24:159–160.
23. van Duijn CM, et al. (2001) Park7, a novel locus for autosomal recessive early-onset parkinsonism, on chromosome 1p36. *Am J Hum Genet* 69:629–634.
24. Clements CM, McNally RS, Conti BJ, Mak TW, Ting JP (2006) DJ-1, a cancer- and Parkinson's disease-associated protein, stabilizes the antioxidant transcriptional master regulator Nrf2. *Proc Natl Acad Sci USA* 103:15091–15096.
25. Joyce BR, Queener SF, Wek RC, Sullivan WJ, Jr. (2010) Phosphorylation of eukaryotic initiation factor-2alpha promotes the extracellular survival of obligate intracellular parasite *Toxoplasma gondii*. *Proc Natl Acad Sci USA* 107:17200–17205.
26. Carruthers VB, Sibley LD (1997) Sequential protein secretion from three distinct organelles of *Toxoplasma gondii* accompanies invasion of human fibroblasts. *Eur J Cell Biol* 73:114–123.
27. Donald RG, Carter D, Ullman B, Roos DS (1996) Insertional tagging, cloning, and expression of the *Toxoplasma gondii* hypoxanthine-xanthine-guanine phosphoribosyltransferase gene. Use as a selectable marker for stable transformation. *J Biol Chem* 271:14010–14019.

Supporting Information

Hall et al. 10.1073/pnas.1105622108

SI Discussion

Uridine phosphorylase (UrdPase) was the top hit from TOP-ABPP (tandem orthogonal proteolysis–activity-based protein profiling) based on spectral counts of the modified peptide. This protein was modified at Cys36 by WRR-086, a residue that is not likely to be an active site residue according to sequence alignments with both the human and *Escherichia coli* proteins. Furthermore, TgUrdPase is involved in the pyrimidine salvage pathway of *Toxoplasma gondii* and is responsible for the nonspecific reversible phosphorolysis of nucleosides and deoxynucleosides (1). Inhibition of this enzyme would therefore likely result in a complete block in pyrimidine salvage. However, *Toxoplasma* is capable of synthesizing pyrimidines de novo. Because this enzyme is involved in DNA replication and intracellular survival, inhibition of this target would be likely to induce effects on the parasite over the timescale of hours. Treatment of extracellular parasites with WRR-086 for 15 min is sufficient to induce a block in parasite attachment to host cells. Therefore, we do not believe that TgUrdPase is a functionally relevant target of WRR-086. The cytosol aminopeptidase on the list is a metalloprotease, and the modified cysteine is not likely to play a direct role in its enzyme activity. The kelch domain protein hit had overall low spectral counts, and GAPDH is an abundant protein involved in the final steps of glycolysis. Recently, TgGAPDH was shown to relocalize to the parasite pellicle during invasion and egress from host cells (2). It has been proposed that this relocalization provides the energy required to drive parasite gliding motility. Although WRR-086 does inhibit gliding motility, the most pronounced phenotype is related to attachment to host cells and microneme secretion, suggesting that WRR-086 acts upstream of the gliding process. Therefore, GAPDH is unlikely to be the functionally relevant protein target of WRR-086.

SI Materials and Methods

High-Throughput Invasion Assay. The assembly of the directed protease inhibitor library was previously reported (3). The library was screened for compounds that block parasite invasion using a previously described high-throughput dual-fluorescence microscopy-based assay (4). Briefly, compounds (50 μM) or vehicle (DMSO) were added to YFP_2 parasites and BS-C-1 Monkey Vero cells in 384-well plate format for 15 min at 25 °C before switching cells to the invasion-permissive temperature of 37 °C for 1 h. After 1 h, cells were washed twice with HH (HBSS supplemented with 10 mM Hepes, pH 7.4), and cells were fixed with 3.5% formaldehyde in 1× PBS for 15 min at 25 °C. After fixing, cells were washed once with 1× HH and blocked in HHB [HBSS supplemented with 10 mM Hepes (pH 7.4) and 3% (wt/vol) BSA] for 1 h at room temperature. Extracellular parasites were next stained with a 1:1,000 dilution of mAb 11-132 in 1× PBS/3% BSA for 15 min at 25 °C followed by a 1:2,500 dilution of Alexa 594-conjugated goat anti-mouse IgG (Invitrogen) in 1× PBS/3% BSA for 15 min at 25 °C. Plates were preserved by the addition of 50 μL 75% (vol/vol) glycerol in PBS per well and stored at 4 °C until imaged. Red and green fluorescence image pairs for five randomly selected fields per compound or vehicle control were captured using the ImageXpress 5000A automated image capture system (Molecular Devices; part of the Stanford University High Throughput Biosciences Center) equipped with a CFP/YFP/HcRed-3X3M-A Triple-band "Sedat" Filter Set for YFP and Alexa 594 fluorescence, and images were viewed using MetaXpress image analysis software. Merged images were scored manually for qualitative differences in the ratio of intracellular (YFP positive, green) to extracellular (YFP positive/Alexa 594 positive, yellow) parasites.

Triaging of Preliminary Hits. Preliminary hits were tested for compound purity using LC/MS (LC, Agilent 1100 series; MC, API 150EX, Applied Biosystems). Seventeen inhibitors were eliminated on the basis of compound impurity as assayed by standard LC-MS methods. All compounds were screened for general toxicity to both host (BS-C-1) cells and parasites (YFP_2) using the CellTiter-Glo luminescent cell viability assay (Promega), and data were collected using a SpectraMax M5 (Molecular Devices). Host cell viability was determined after a 24-h compound treatment (50 μM final concentration), and parasite viability was determined after a 1-h compound treatment (50 μM) using extracellular parasites. No inhibitors were found to be generally toxic to the parasites or host cells under these assay conditions. In addition to ATP production assays, toxicity to host cells was further determined by microscopic analysis of changes in host cell morphology after a 24-h compound treatment. Five additional inhibitors were eliminated owing to gross morphological changes of host cells after compound treatment. Finally, we determined the reversible nature of the compounds on parasite invasion. To do this, parasites and host cells were treated with compound or vehicle independently, washed to remove excess compound, and then combined (inhibitor-treated parasites/vehicle-treated host cells, vehicle-treated parasites/inhibitor-treated host cells) to determine (*i*) whether the compound was affecting parasite-derived or host cell-derived proteins and (*ii*) whether the compound produced an irreversible inhibition of host cell invasion.

Quantitative ENDO-Synchronized Invasion/Attachment Assay. Human foreskin fibroblasts (HFFs) were grown to confluency on glass coverslips in 24-well plates for 24–48 h. Just before the invasion assay, HFF monolayers were washed three times with 1× PBS, and media was replaced with Endo buffer (44.7 mM K_2SO_4, 10 mM $MgSO_4$, 106 mM sucrose, 5 mM glucose, 20 mM Tris-H_2SO_4, and 3.5 mg/mL BSA). Parasites were pretreated with compound or vehicle for 15 min at 25 °C and washed by centrifugation (1,200 × *g*, 5 min) to remove excess compound. Washed parasites were resuspended in Endo buffer and added to HFF monolayers for 30 min at 37 °C. Endo buffer was replaced with normal invasion media [DMEM, 1% dialyzed FBS (dFBS)], and parasites were allowed to invade host cells for 20 min at 37 °C, after which time cells were washed once with 1× PBS and fixed with 3.5% formaldehyde in PBS for 15 min at room temperature. Cells were washed once with 1× PBS, and extracellular parasites were stained as described above with the following modifications made for assays that did not use fluorescent parasites. After fixing and blocking, extracellular parasites were stained with a 1:1,000 dilution of mAb 11–132in 1× PBS/3% (wt/vol) BSA for 1 h. Host cells and parasites were then permeabilized by the addition of 100% ethanol for 10 min at 25 °C. Monolayers were washed 3 × 5 min with 1× PBS, and then all parasites were stained with a 1:5,000 dilution of a polyclonal rabbit anti-SAG1 in 3% BSA/1× PBS/0.02% Triton X-100 for 1 h. Monolayers were washed 5 × 5 min with 1× PBS, followed by the addition of a mixture of Alexa 594-conjugated goat anti-mouse IgG and Alexa 488-conjugated goat anti-rabbit IgG (each 1:5,000 in 3% BSA/0.02% Triton X-100 in 1× PBS) for 1 h. Monolayers were washed 5 × 5 min, coverslips were mounted over 3 μL of Vectashield mounting medium, and slides were stored at 4 °C until imaged.

Ten randomly selected fields were scored manually for the number of extracellular and intracellular parasites. Attachment efficiency was calculated as the average number of total parasites (extracellular plus intracellular) from compound-treated samples

divided by the average number of total parasites per field from vehicle-treated samples. Invasion efficiency was calculated as the average percentage of compound-treated invaded parasites (number of invaded parasites/number of total parasites per field) divided by the average percentage of vehicle-treated invaded parasites. Phase and fluorescence images were captured on a Hamamatsu Orca100 CCD camera coupled to an Olympus BX60 microscope and were processed using Image-Pro Plus 2.0 (Media-Cybernetics) and Photoshop CS4 (Adobe Systems).

All data were analyzed using nonlinear regression analysis in KaleidaGraph using a logistic response model curve fit [curve fit definition: $100/(1 + \exp(m2 \times (m0 - m1)))$; $m1 = -5$; $m2 = 2$]. Effector concentrations for EC_{50} were then calculated using Derive.

Assessment of *Toxoplasma* Replication by FACS. Confluent monolayers of HFFs grown in 24-well plates were washed once with HBSS before infection with 5×10^4 RH-GFP parasites in Endo buffer (to facilitate synchronized invasion). Parasites were allowed to settle for 30 min at 37 °C before removal of Endo buffer, followed by the addition of invasion media (DMEM supplemented with 1% dFBS) and incubation for 20 min at 37 °C to allow parasites to invade. Noninvaded parasites were removed by three sequential washes with HBSS before the addition of DMEM with varying concentrations of WRR-086 (0–50 μM). Intracellular replication was allowed to proceed for 28 h before detachment of the HFF monolayer with trypsin and fixing in 4% formaldehyde/PBS before FACS analysis.

FACS analysis was conducted on an LSRII (BD Biosciences) flow cytometer in the Stanford Shared FACS facility and analyzed using FlowJo (Treestar). The mean fluorescence intensity of the GFP-positive (*Toxoplasma*-infected) host cells was divided by the mean fluorescence intensity of the free parasite population to give an approximate number of parasites per infected host cell. Data are presented as the average of triplicate experiments. In all conditions the total proportion of GFP-positive cells was 4.5–5%, indicating that little further invasion had occurred during the intracellular growth phase of the experiment.

Solid-Phase Synthesis of WRR-086 and Analogs. Dry Weinreb amide resin (0.88 mmol/g) was weighed into polypropylene cartridges (Applied Separations). Columns were fitted with Teflon stopcocks (BioRad Laboratories) and connected to a 20-port vacuum manifold (Waters) used to drain reagents and solvents from the resin. Resins were swelled using dimethylformamide (DMF) for 3 min, followed by deprotection of the Fmoc protecting group using 20% piperidine in DMF for 15 min with rotation. Fmoc-Ala (28.02 mg, 90 μmol, 3 eq), 2-(1H-7-Azabenzotriazol-1-yl)–1,1,3,3-tetramethyl uronium hexafluorophosphate Methanaminium (33.08 mg, 87 μmol, 2.9 eq), and N,N-Diisopropylethylamine (26.12 μL, 150 μmol, 5 eq) were dissolved in 360 μL DMF, added to the resin, and agitated overnight. The resin was washed, and the N-terminal Fmoc group was deprotected. Fmoc-Phe (34.87 mg, 90 μmol, 3 eq), N-Hydroxybenzotriazole (12.16 mg, 90 μmol, 3 eq), and N,N'-diisopropylcarbodiimide (14.01 μL, 90 μmol, 3 eq) were dissolved in 360 μL DMF, added to the resin, and agitated for 2 h. Resin was washed, and the Fmoc group was deprotected. Z-Osu (22.43 mg, 90 μmol, 3 eq) and N,N-Diisopropylethylamine (26.13 μL, 150 μmol, 5 eq) were dissolved in 260 μL DMF, added to the resin, and agitated for 2 h. Resins were washed three times with DMF, three times with dichloromethane, and then lyophilized for 1 h to dryness. Resins were washed three times with dry tetrahydrofuran (THF) and drained. Five hundred forty microliters of 1 M vinyl magnesium bromide (15 eq) and 660 μL of dry THF (0.025 M final concentration) were added to the resin, and the resin was agitated at room temperature overnight (for at least 13 h). Resins were drained, the inhibitor was cleaved from the resin by the addition of 1 mL of cleavage mixture (5% TFA/15% water/2.5% triisopropylsilane in dry THF), and the resin was agitated for 10 min. The solution was collected in a clean, dry, round-bottom flask, the resin was washed again briefly with an additional 1 mL of the cleavage mixture, and the wash was collected in the same round-bottom flask. The crude product was rotavapped to dryness and then redissolved in 1 mL of dry DMSO. The product was purified on a C18 reverse-phase HPLC column (Waters, Delta-Pak) using a linear gradient of 0–100% water-acetonitrile. Fractions containing the product were pooled, frozen, and lyophilized to dryness. Compound identity and purity were assessed by LC-MS analysis (see below).

All analogs were synthesized using the same conditions as described above with the exception of WRR-086-Ctrl, which was synthesized with the following modification. The vinyl magnesium bromide Grignard reagent was replaced with ethyl magnesium bromide. All other aspects of the synthesis remained the same.

Microneme Secretion. Microneme secretion was assayed as previously described (5), with the following modifications. Syringe-lysed and filtered parasites were washed in 10 mL cold HH (pH 7.0) and then resuspended in secretion media [HBSS containing 20 mM Hepes (pH 7.0) and 1% (vol/vol) dFBS)] at 4.0×10^8 parasites/mL. Parasites (100 μL) were pretreated with vehicle, BAPTA-AM [1,2-bis-(*o*-Aminophenoxy)-ethane-N,N,N',N'-tetraacetic acid, tetraacetoxymethyl ester; final concentration of 20 μM], or compound at the indicated concentrations for 15 min at room temperature to mimic the compound treatment used in the invasion assays described above. Excess compound was washed away by centrifugation ($1,200 \times g$, 5 min), and washed parasites were resuspended in 100 μL secretion media without compound (except for BAPTA-AM, which was reintroduced at a final concentration of 20 μM because BAPTA-AM is a reversible calcium chelator). To detect constitutive secretion, parasites were then incubated at 37 °C for 30 min. To detect induced secretion, parasites were treated with 1% (vol/vol) ethanol at 37 °C for 4 min. After secretion, parasites were incubated on ice for 5 min to stop microneme secretion, and then parasites were pelleted ($1,200 \times g$, 5 min, 4 °C). Ninety-five microliters of supernatant was transferred to a new Eppendorf tube and recentrifuged ($1,200 \times g$, 5 min, 4 °C). Ninety microliters of this supernatant was transferred to a new Eppendorf tube and was dissolved with reducing SDS/PAGE sample buffer. Proteins were separated on a 2–8% NuPAGE Novex Tris-Acetate precast gel (Invitrogen), and the presence of MIC2 was detected by Western blotting with a mouse monoclonal antibody against MIC2 (1:5,000; kind gift from Vern Carruthers, University of Michigan, Ann Arbor, MI) (5), followed by an HRP-conjugaged goat anti-mouse antibody (1:5,000; KPL). As a control for starting with equal parasite numbers, the parasite pellets were resuspended in 2× reducing SDS sample buffer, boiled, and proteins were separated on 15% polyacrylamide gels and analyzed for the presence of the surface antigen, SAG1, with a mouse monoclonal antibody, DG52 (1:100), followed by an ECL HRP-conjugated goat anti-mouse secondary antibody (1:1,000). All EC_{50} values were calculated as described above.

Gliding Motility/Trail Deposition Assays. Trail deposition/gliding motility were assayed as previously described (4), with the following modifications. Freshly harvested and syringe-filtered parasites were treated for 15 min with varying concentrations of WRR-086, the inactive control compound WRR-086-Ctrl, or vehicle, after which time excess compound was removed by centrifugation ($1,200 \times g$, 5 min, 25 °C). Parasites were resuspended in Endo buffer and allowed to settle onto FBS-coated coverslips in 24-well plates for 20 min at 37 °C to synchronize gliding motility. After 20 min, Endo buffer was replaced with HHdF [HBSS, 20 mM Hepes (pH 7.0), 1% (vol/vol) dFBS], and parasites were allowed to glide for 15 min at 37 °C. Coverslips were washed and then fixed with 3.5% formaldehyde/1× PBS for 15 min at 25 °C.

Coverslips were blocked with 3% (wt/vol) BSA in 1× PBS for 1 h, and SAG1 trails were visualized by staining with a 1:1,000 dilution of mAb 11-132 in 3% BSA (wt/vol)/1× PBS, followed by a 1:2,500 dilution of Alexa 488-conjugated goat anti-mouse IgG in 3% BSA (wt/vol)/1× PBS. Coverslips were prepared, and images were captured and analyzed as described above.

Target Identification by TOP-ABPP. Freshly lysed and syringe-filtered parasites were pretreated with vehicle or WRR-086 (50 μM) for 30 min and then labeled intact with 5 μM of alkyne-086 for 1 h at room temperature. Excess compound was removed by centrifugation (1,200 × *g*, 5 min, 25 °C), and parasites were resuspended in lysis buffer (1% Nonidet P-40 in 1× PBS, pH 7.0) and incubated on ice for 2 h. Parasite debris and insoluble proteins were removed by centrifugation, and lysates were diluted to 2 mg/mL total protein and flash-frozen in liquid nitrogen and stored at −80 °C until enough protein was collected for TOP-ABPP.

Protein labeling and click chemistry. Proteome samples were diluted to a 1 mg protein/mL solution in PBS. Click chemistry was performed on each sample (2 × 0.5 mL aliquots) by the addition of 100 μM of the TEV-biotin tag [50× stock in DMSO, synthesis reported previously (6)], 1 mM tris(2-carboxyethyl)phosphine (TCEP) (fresh 50× stock in water), 100 μM ligand (17× stock in DMSO:t-Butanol 1:4), and 1 mM $CuSO_4$ (50× stock in water). Samples were allowed to react at room temperature for 1 h. Tubes were combined pairwise and centrifuged (5,900 × *g*, 4 min, 4 °C) to pellet the precipitated proteins. The pellets were resuspended in cold MeOH by sonication and tubes combined pairwise. Centrifugation was followed by a second methanol wash, after which the pellet was solubilized in PBS containing 1.2% SDS via sonication and heating (5 min, 80 °C).

Streptavidin enrichment of probe-labeled proteins. The SDS-solubilized, probe-labeled proteome samples were diluted with 5 mL of PBS for a final SDS concentration of 0.2%. The solutions were then incubated with 100 μL of streptavidin-agarose beads (Pierce) for 3 h at room temperature. The beads were washed with 10 mL 0.2% SDS/PBS, 3 × 10 mL PBS, and 3 × 10 mL H_2O and the beads were pelleted by centrifugation (1,300 × *g*, 2 min) between washes.

On-bead trypsin and TEV digestion. The washed beads from above were suspended in 500 μL of 6 M urea/PBS and 10 mM TCEP (from 20× stock in H_2O) and placed in a 65 °C heat block for 15 min. Iodoacetamide (20 mM; from 50× stock in H_2O) was then added and allowed to react at 37 °C for 30 min. After reduction and alkylation, the beads were pelleted by centrifugation (1,300 × *g*, 2 min) and resuspended in 150 μL of 2 M urea/PBS, 1 mM $CaCl_2$ (100× stock in H_2O), and trypsin (2 μg). The digestion was allowed to proceed overnight at 37 °C. The tryptic digest was separated from the beads using a Micro Bio-Spin column and saved for MS analysis. The beads were then washed with 3 × 500 μL PBS, 3 × 500 μL H_2O, and 1 × 150 μL of TEV digest buffer. The washed beads were then resuspended in 150 μL of TEV digest buffer with AcTEV Protease (Invitrogen; 5 μL) for 12 h at 29 °C. The eluted peptides were separated from the beads using a Micro Bio-Spin column and the beads washed with H_2O (2 × 75 μL). Formic acid (15 μL) was added to the sample, which was stored at −20 °C until MS analysis.

LC-MS analysis. LC-MS analysis was performed on an LTQ ion trap mass spectrometer (ThermoFisher) coupled to an Agilent 1100 series HPLC. Tryptic and TEV digests were pressure-loaded onto a 250-μm fused silica desalting column packed with 4 cm of Aqua C18 reverse-phase resin (Phenomenex). The peptides were then eluted onto a biphasic column (100 μm fused silica with a 5-μm tip, packed with 10 cm C18 and 3 cm Partisphere strong cation exchange resin; SCX, Whatman) using a gradient 5–100% buffer B in buffer A (buffer A: 95% water, 5% acetonitrile, 0.1% formic acid; buffer B: 20% water, 80% acetonitrile, 0.1% formic acid). The peptides were then eluted from the SCX onto the C18 resin and into the mass spectrometer using the salt steps previously reported (6, 7). The flow rate through the column was set to ≈0.25 μL/min, and the spray voltage was set to 2.75 kV. One full MS scan (400–1,800 MW) was followed by 18 data-dependent scans of the n^{th} most intense ions with dynamic exclusion disabled.

MS data analysis. The generated tandem MS data were searched using the SEQUEST algorithm against a combined human-*Toxoplasma* database. A static modification of +57 on Cys was specified to account for iodoacetamide alkylation. For the TEV digests, a differential modification of +555.3 was specified on Cys. SEQUEST output files were filtered using DTASelect with default parameters as described in the DTASelect manual v1.9 [min Xcorr = 1.8 (+1), 2.5 (+2), 3.5 (+3), min DeltaCN = 0.08]. Reported peptides were also required to be fully tryptic and contain the desired probe modification.

Sequence Alignment and Homology Modeling of TgDJ-1. DJ-1 sequences were aligned using CLUSTALW (8). A model of the TgDJ-1 structure was created from the YopJ structure (9) (Protein Data Bank ID: 2AB0) using Modeler (10). The homology model for *T. gondii* DJ-1 in Fig. S3 was built from the crystal structure of *Pyrococcus horikoshii* PH1704 (Protein Data Bank ID: G2I; PubMed ID: 11114201), which shares 28% identity and 47% similarity with TGME49_014290. This protease is composed of six identical subunits arranged in a symmetrical ring configuration, with three active sites situated at the interface between subunits. After aligning the predicted sequence of TGME49_014290 (ToxoDB) with that of PH1704, a hexameric model of *T. gondii* DJ1 was built using the default parameters of the molecular modeling program MOE (Chemical Computing Group). Each subunit of *T. gondii* DJ1 contains six cysteine residues, none of which are positioned close enough to form intra- or intersubunit disulfide bonds.

Expression of Recombinant TgDJ-1 Proteins. The TgDJ-1 coding sequence was amplified directly from *T. gondii* strain RH1 cDNA and cloned into the pET-15 expression vector with 5′ *Nde* 1 and 3′ *Eco* R1 restriction enzyme sites in frame with the N-terminal His6 tag for later purification. C104A and C127A mutations were introduced into the WT pET15-TgDJ-1 expression construct using the Stratagene QuikChange site-directed mutagenesis strategy, and successful mutagenesis was confirmed by sequencing of selected clones. pET15-TgDJ-1, pET15-TgDJ-1/C104A, and pET15-TgDJ-1/C127A expression constructs were transformed into *E. coli* BL21-DE3s and single clones picked for overnight cultures. After inoculation from a turbid culture, 50-mL bacterial cultures were grown until OD_{600} = 0.8. Expression was induced with 0.25 mM isopropyl-beta-D-1-thiogalactopyranoside (IPTG) for 3 h at 37 °C. Induced cultures were pelleted and the recombinant proteins purified by standard nickle-chelate chromatography. Purified proteins were dialyzed overnight at 4 °C against 50 mM Tris-HCl (pH 8), 200 mM NaCl, and 5 mM $CaCl_2$, then concentrated and snap-frozen until required. Fifty milliliters of induced bacterial cultures typically yielded 1 mg of recombinant TgDJ-1.

WRR-086-Biotin Labeling Assay. Freshly egressed extracellular tachyzoites were harvested and washed with 5 mL PBS. Approximately 20 μL of pelleted, washed tachyzoites were lysed with 200 μL of lysis buffer [50 mM Tris-HCl (pH 8), 200 mM NaCl, 5 mM $CaCl_2$, 0.1% SDS, and 1% Nonidet P-40] for 5 min on ice. The lysed sample was then centrifuged at 16,000 × *g* in a benchtop microfuge for 15 min at 4 °C. The protein concentration of the clarified lysate supernatant was measured and was typically 2 mg/mL. Labeling assays were performed as follows: 500 ng of recombinant protein (WT/C104A/C127A) was spiked into 20 μg *T.*

gondii lysate and labeled with 1 μM WRR-086_biotin for 15 min at 4 °C. Samples were solublilized with 20 μL 2× reducing SDS sample buffer and fractionated by SDS/PAGE. Duplicate gels were run: one gel was stained with Coomassie to control for equal protein quantity between samples and the second transferred onto nitrocellulose membrane. After transfer, membranes were blocked and probed with a streptavidin-HRP conjugate (Sigma) and imaged by standard autoradiography.

1. Iltzsch MH, Klenk EE (1993) Structure-activity relationship of nucleobase ligands of uridine phosphorylase from *Toxoplasma gondii*. *Biochem Pharmacol* 46:1849–1858.
2. Pomel S, Luk FC, Beckers CJ (2008) Host cell egress and invasion induce marked relocations of glycolytic enzymes in *Toxoplasma gondii* tachyzoites. *PLoS Pathog* 4: e1000188.
3. Arastu-Kapur S, et al. (2008) Identification of proteases that regulate erythrocyte rupture by the malaria parasite *Plasmodium falciparum*. *Nat Chem Biol* 4:203–213.
4. Carey KL, Westwood NJ, Mitchison TJ, Ward GE (2004) A small-molecule approach to studying invasive mechanisms of *Toxoplasma gondii*. *Proc Natl Acad Sci USA* 101: 7433–7438.
5. Carruthers VB, Giddings OK, Sibley LD (1999) Secretion of micronemal proteins is associated with toxoplasma invasion of host cells. *Cell Microbiol* 1:225–235.
6. Weerapana E, Speers AE, Cravatt BF (2007) Tandem orthogonal proteolysis-activity-based protein profiling (TOP-ABPP)—a general method for mapping sites of probe modification in proteomes. *Nat Protoc* 2:1414–1425.
7. Speers AE, Adam GC, Cravatt BF (2003) Activity-based protein profiling in vivo using a copper(i)-catalyzed azide-alkyne [3 + 2] cycloaddition. *J Am Chem Soc* 125: 4686–4687.
8. Larkin MA, et al. (2007) Clustal W and Clustal X version 2.0. *Bioinformatics* 23: 2947–2948.
9. Wilson MA, Ringe D, Petsko GA (2005) The atomic resolution crystal structure of the YajL (ThiJ) protein from *Escherichia coli*: A close prokaryotic homologue of the Parkinsonism-associated protein DJ-1. *J Mol Biol* 353:678–691.
10. Sali A, Blundell TL (1993) Comparative protein modelling by satisfaction of spatial restraints. *J Mol Biol* 234:779–815.

Characterization of compounds:
LC/MS Data
JCP-234 (**1**) – From Library

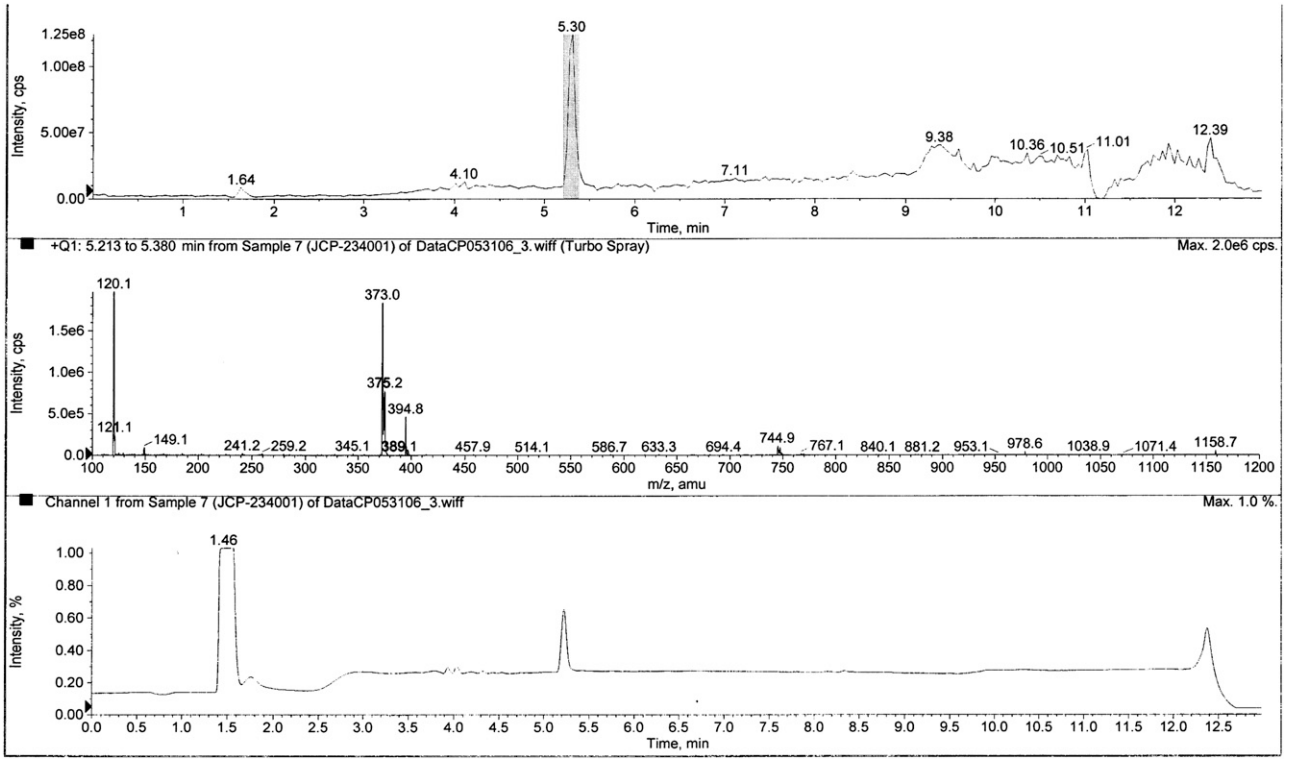

JCP-241 (**2**) – From Library

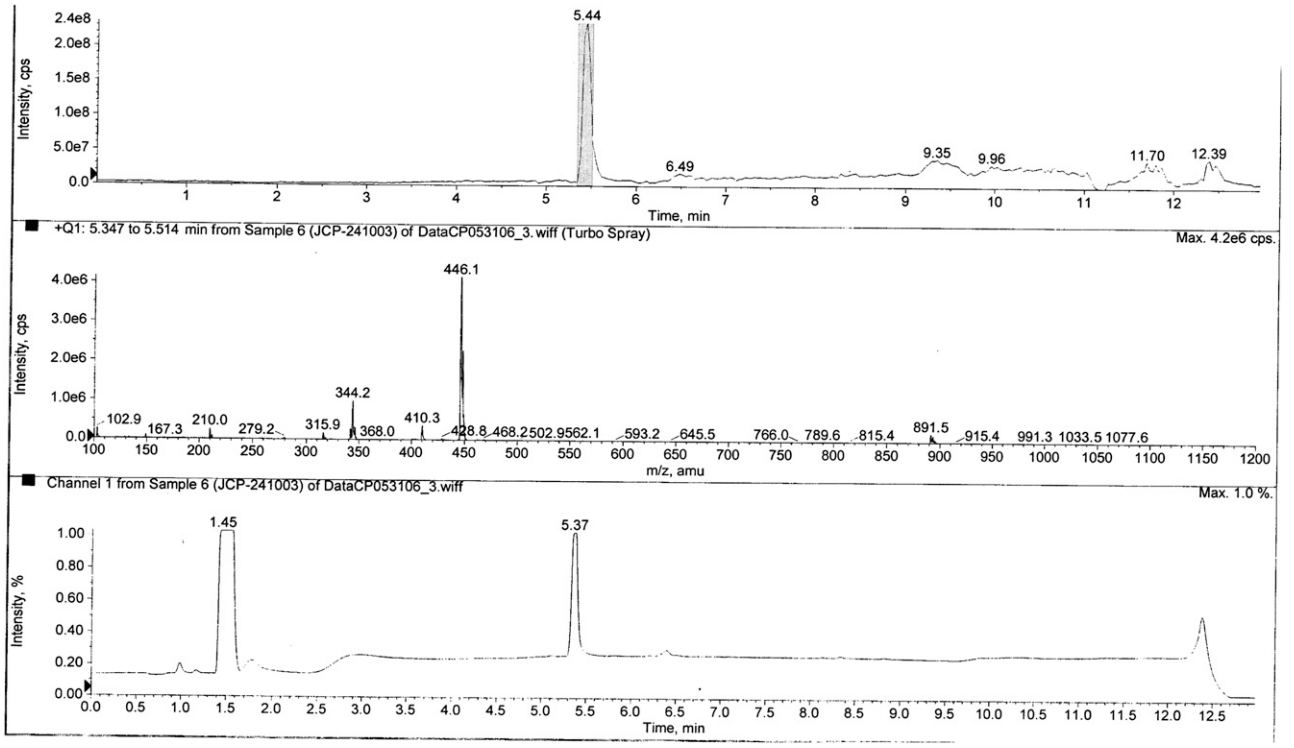

JCP-270 (**3**) – From Library

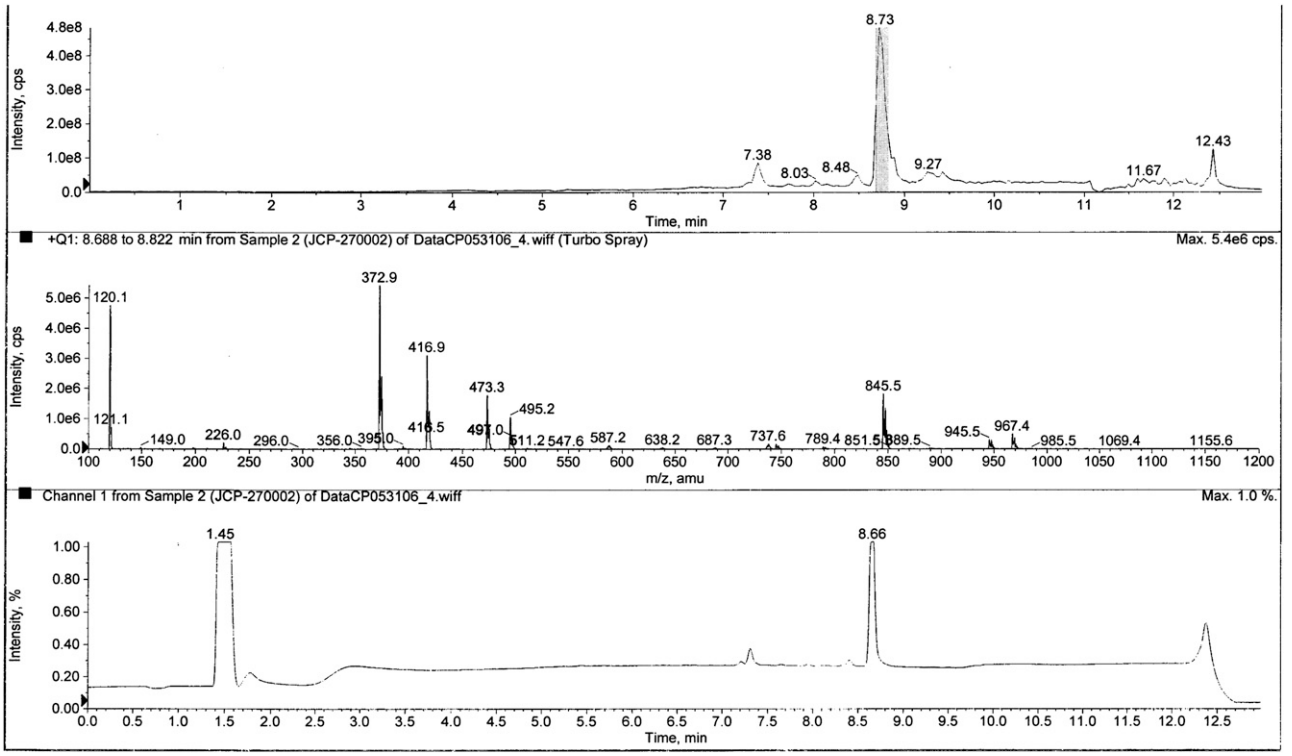

WRR-086 (**4**) – from Library

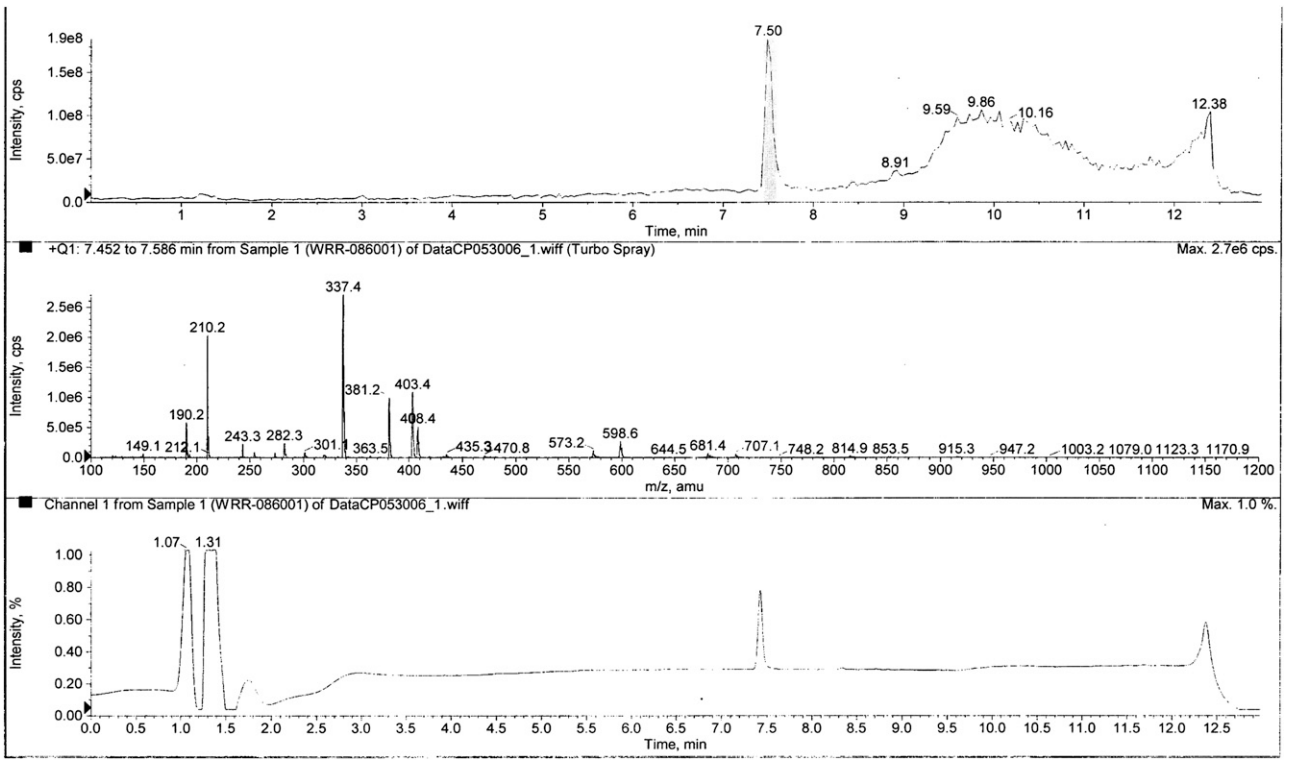

WRR-086 (**4**) – From solid phase synthesis

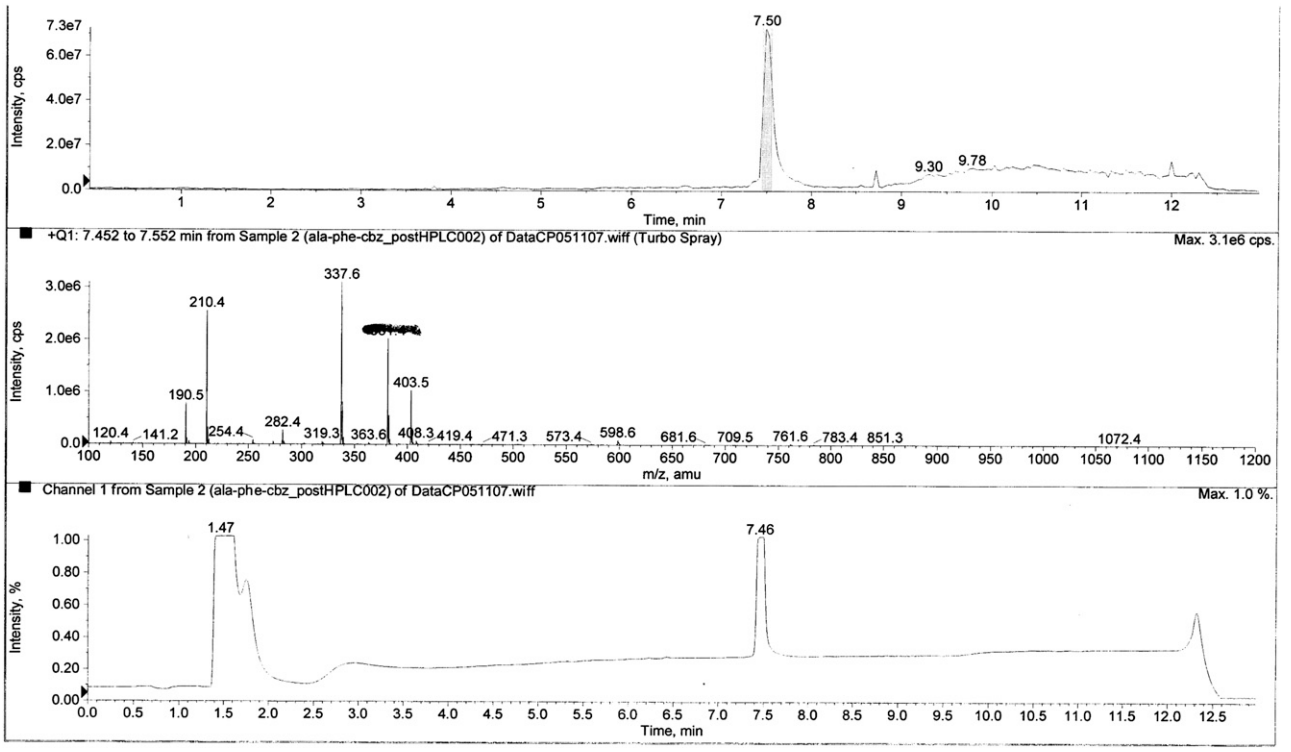

WRR-315 (**5**) – From Library

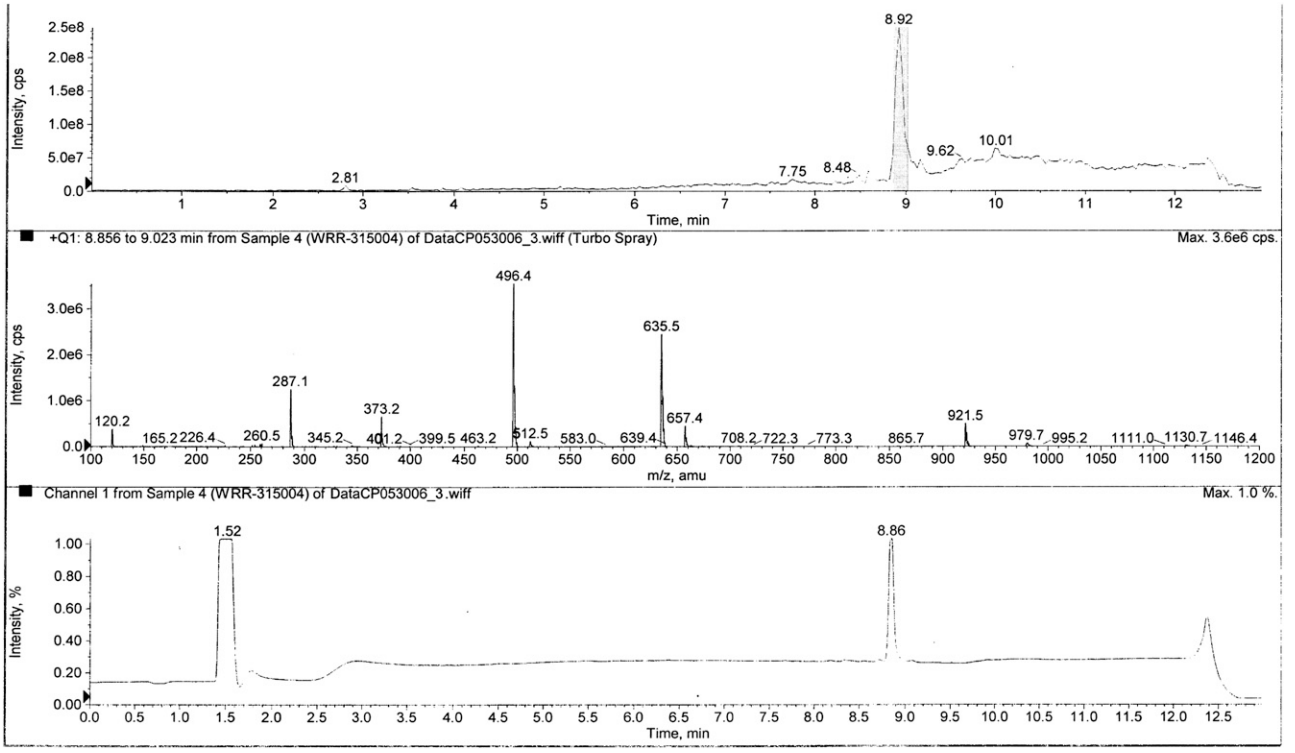

WRR-086-Ctrl (**6**) – From solid phase synthesis

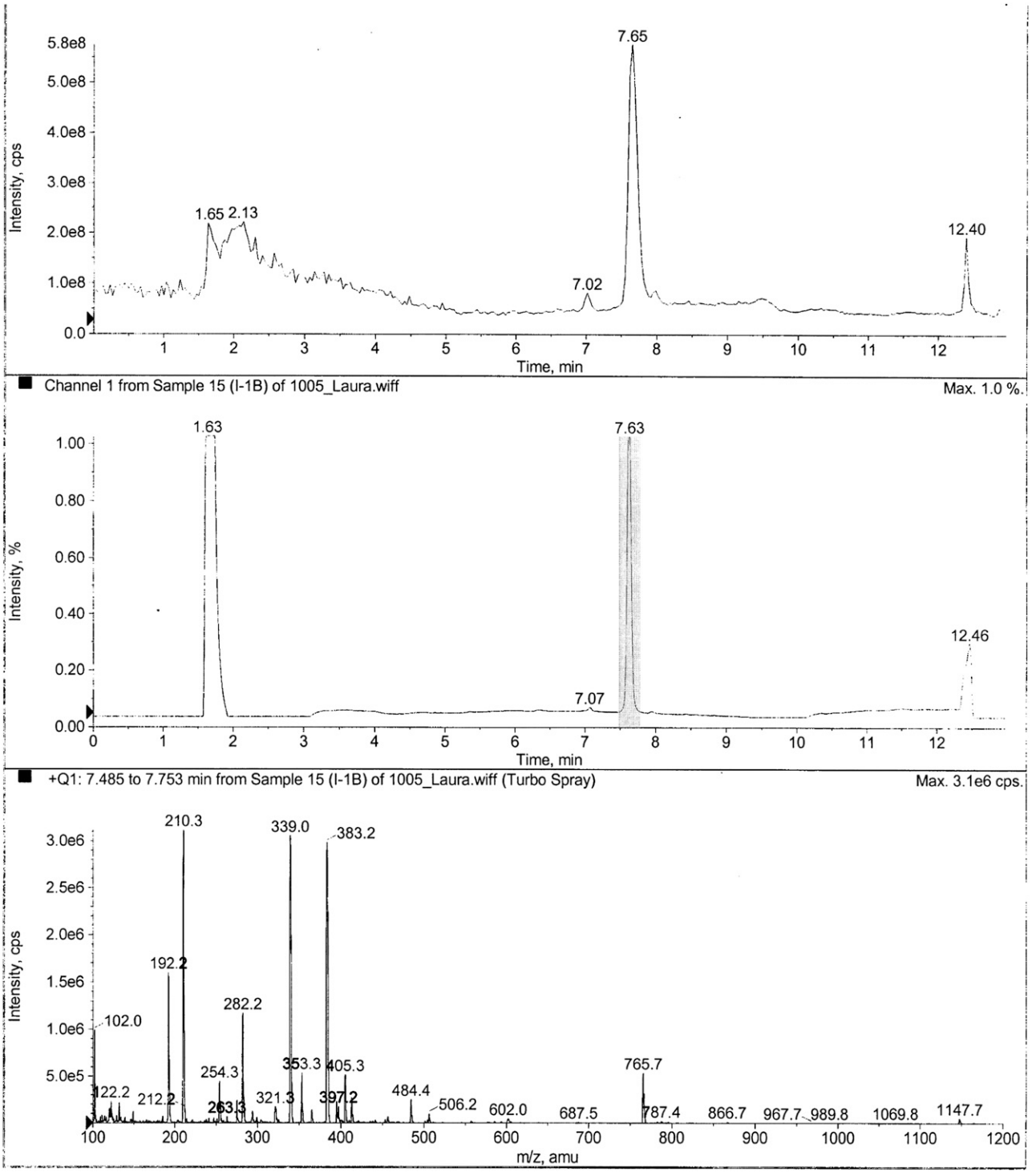

Alkyne-086 (**12**) – From solid phase synthesis

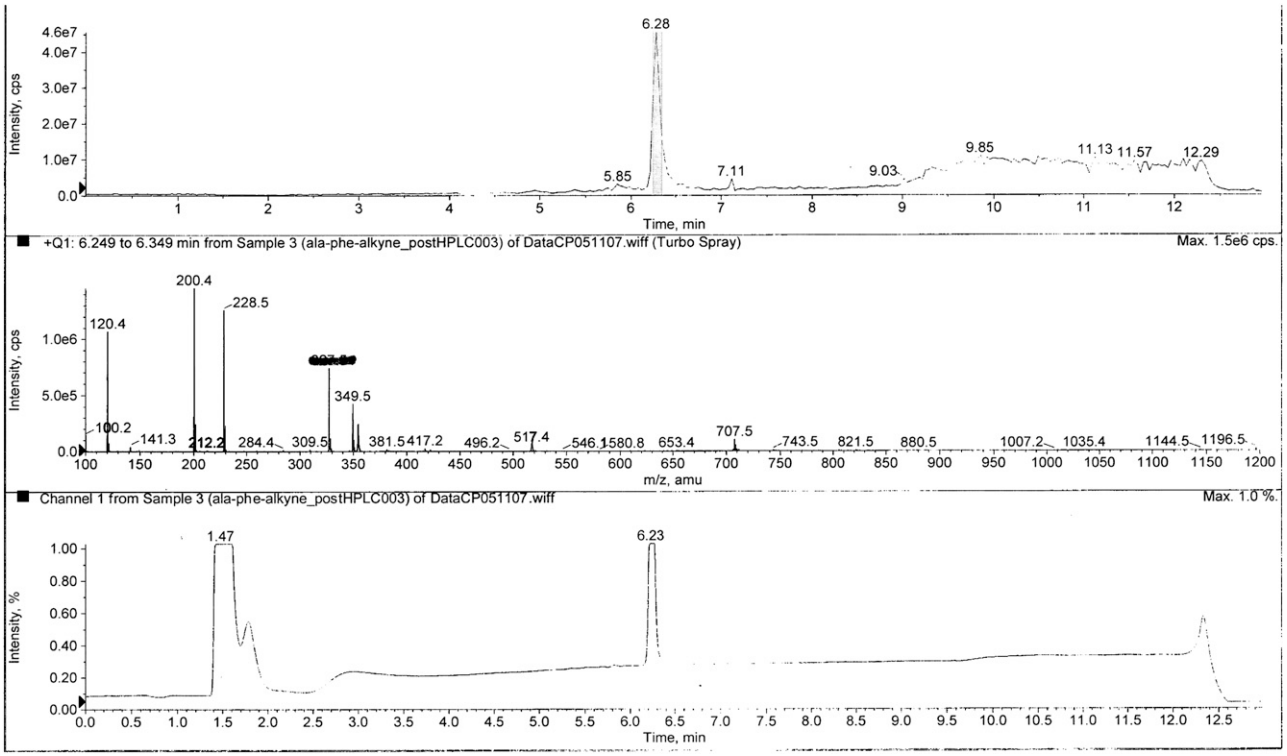

HRMS Data:

WRR-086 (**4**) [MH]+ calcd for C22H25N2O4, 381.1814; found 381.1801.

WRR-086-Ctrl (**6**) [MH]+ calcd for C22H26N2O4Na, 405.1790; found 405.1784.

Alkyne-086 (**12**) [MH]+ calcd for C19H22N2O3Na, 349.1528; found 349.1515.

NMR Data:

WRR-086 (**4**) ^{1}H NMR (400 MHz, DMSO): δ 8.46 (d, 1H, J = 7.2 Hz), 7.54 (d, 1H, J = 8.8 Hz), 7.33–7.17 (m, 10H), 6.47 (dd, 1H, J = 17.6, 10.8 Hz), 6.25 (dd, 1H, J = 17.6, 1.6 Hz), 5.81 (dd, 1H, J = 10.8, 1.6 Hz), 4.92 (s, 2H), 4.54 (dq, 1H, J = 7.2, 7.2 Hz), 4.26 (ddd, 1H, J = 10.8, 8.8, 4.4 Hz), 2.97 (dd, 1H, J = 14.0, 4.4 Hz), 2.71 (dd, 1H, J = 14.0, 10.8 Hz), 1.20 (d, 3H, J = 7.2 Hz).

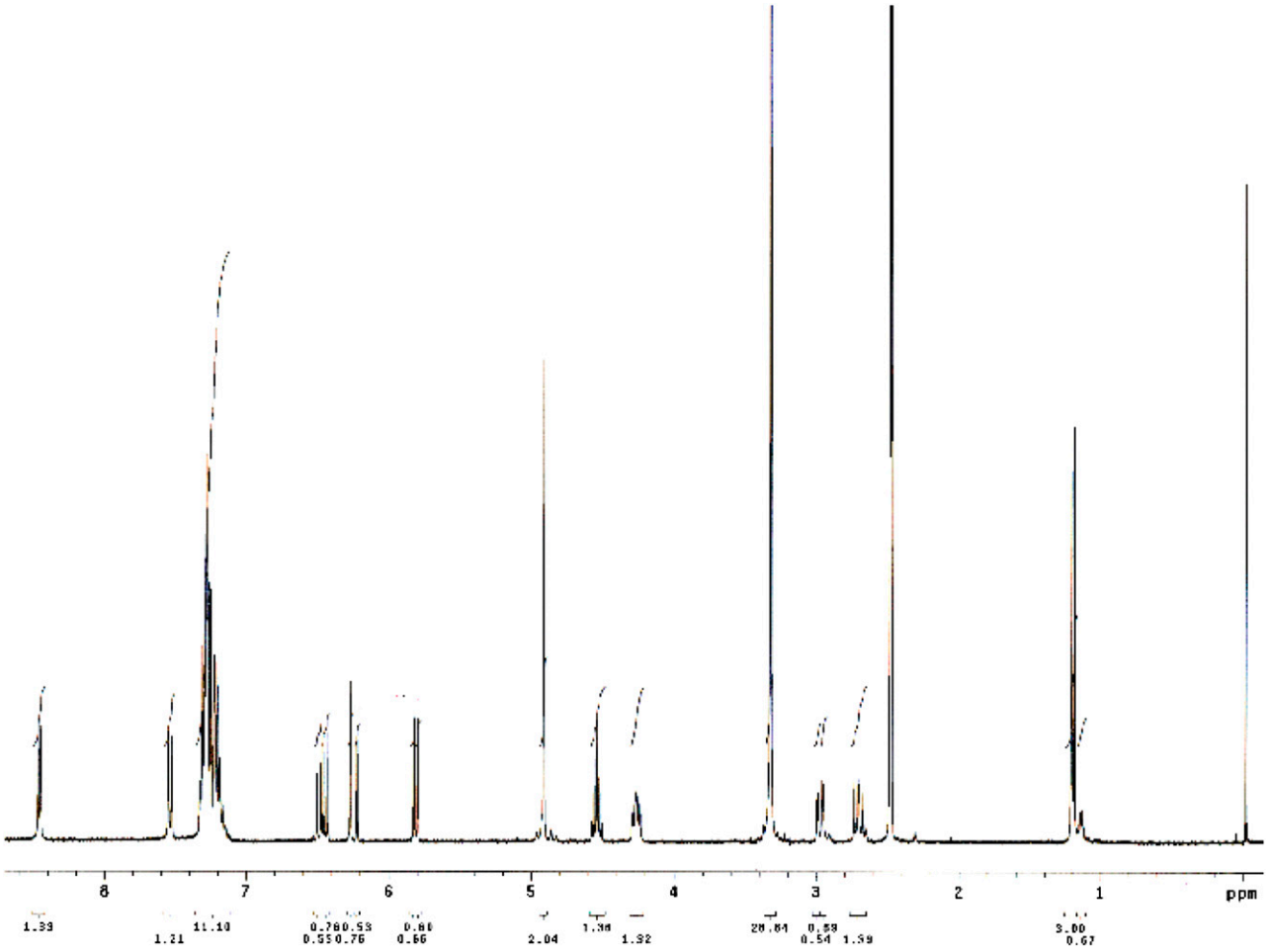

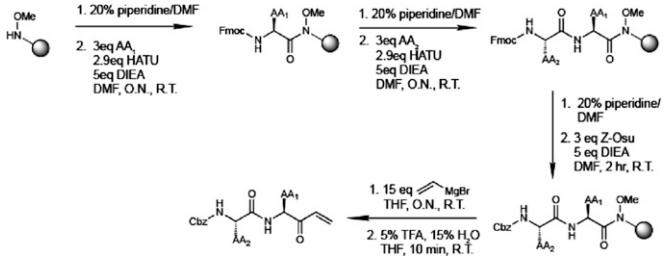

Fig. S1. Solid-phase synthesis of WRR-086 and related analogs. Schematic of solid-phase synthesis of WRR-086, WRR-086-Ctrl, and Alkyne-WRR-086 beginning with Wienreb amide resin. For details of synthesis refer to *SI Materials and Methods*. DMF, dimethylformamide; AA, amino acid; DIEA, N,N-Diisopropylethylamine; O.N., overnight; R.T., room temperature; THF, tetrahyrdofuran; TFA, trifluoroacetic acid.

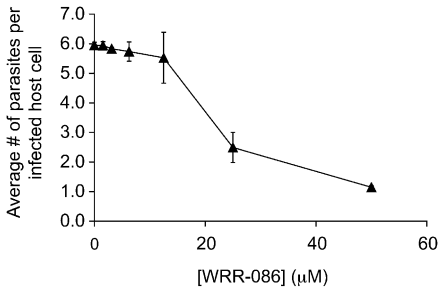

Fig. S2. Effect of WRR-086 on intracellular replication. Confluent monolayers of HFFs were infected with RH-GFP parasites using Endo-synchronization. Parasites were allowed to invade host cells, followed by removal of extracellular parasites. Media containing the indicated concentrations of WRR-086 was added to the infected monolayers, and parasites were allowed to replicate for 28 h before FACS analysis. The mean fluorescence intensity of the GFP-positive (*Toxoplasma*-infected) host cells relative to the free parasite population provides an approximate number of parasites per infected cell. Data are mean values of three independent experiments ± SEMs.

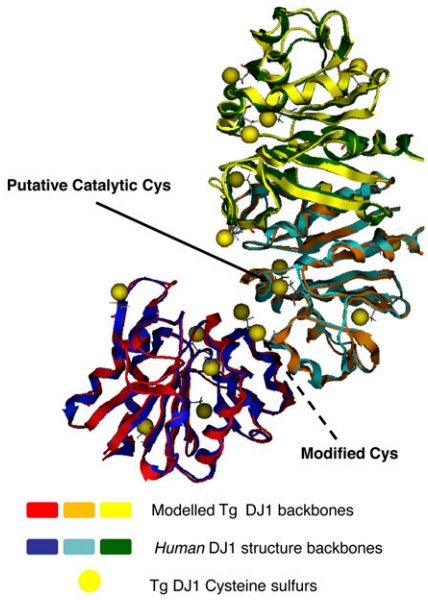

Fig. S3. Homology model of *T. gondii* DJ-1. The model (backbones shown in red, orange, and yellow) was built based on the crystal structure of *Pyrococcus horikoshii* PH1704 (blue, cyan, and green backbones), which is made up of six identical subunits arranged in a symmetric hexameric ring. Three of the six subunits are shown to highlight the two protein–protein interfaces of each monomer with its adjacent subunits. None of the cysteines (sulfur atoms are highlighted in yellow) are close enough to form disulfide bonds. The two closest cysteine residues (3.6 Å apart) are the predicted catalytic cysteine (solid arrow) and Cys127 (dashed arrow).

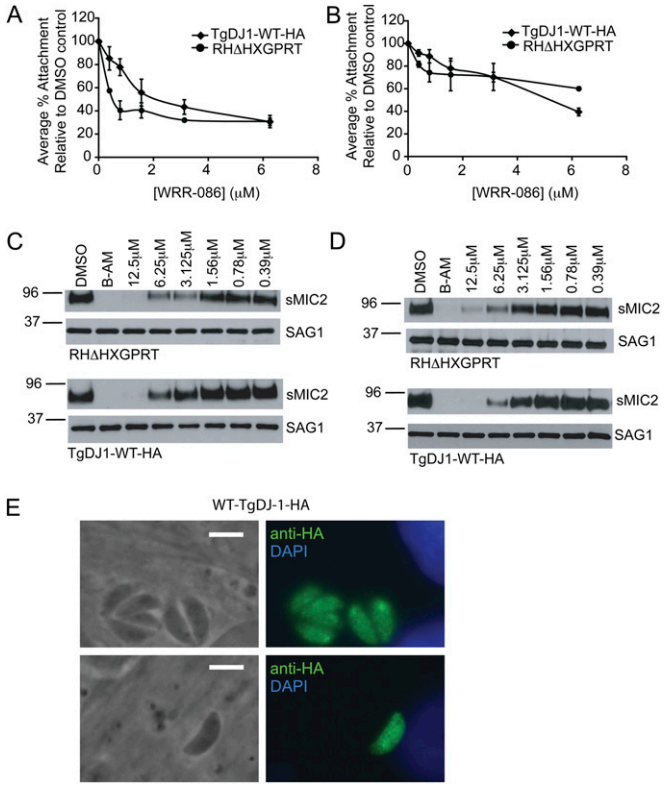

Fig. S4. HA-tagged TgDJ-1 is sensitive to WRR-086 treatment and has diffuse cytsolic localization. (*A* and *B*) Dose–response of WRR-086 against attachment (*A*) and invasion (*B*) of WT (RHΔHXGPRT) parasites compared with parasites expressing TgDJ-1 WT-HA. Parasites were pretreated with vehicle (DMSO) or WRR-086 at the indicated concentrations for 15 min at 25 °C before performing the Endo-synchronized attachment/invasion assay. Data represent mean values ± SEMs of three independent experiments and are expressed as percentages of solvent-treated controls. (*C* and *D*) Effect of WRR-086 on constitutive (*C*) and ethanol-induced (*D*) secretion of MIC2 in WT (RHΔHXGPRT) parasites and TgDJ-1 WT-HA expressing parasites. (*E*) Parasites expressing a WT copy of the DJ-1 gene fused to a C-terminal HA tag were fixed and stained with an anti-HA antibody and DAPI. Representative bright-field and fluorescent images are shown for both intracellular (*Upper*) and extracellular (*Lower*) tachyzoites.

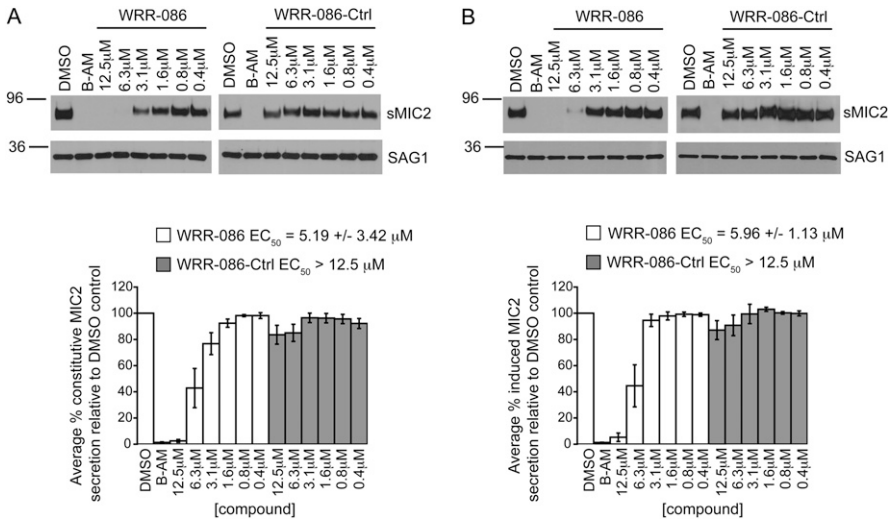

Fig. S5. Dose–response of WRR-086 and WRR-086-Ctrl in constitutive and ethanol-induced microneme secretion. Extracellular tachyzoites were pretreated with vehicle (DMSO), BAPTA-AM, or varying concentrations of WRR-086 and WRR-086-Ctrl as indicated for 15 min, and excess inhibitor was removed by centrifugation. Parasites were left untreated (*A*) or treated with 1% vol/vol ethanol (*B*) and incubated at 37 °C for 4 min, and secretion was stopped by incubation of the parasites on ice for 5 min. Culture supernatants were separated from the parasites by centrifugation, and the amount of MIC2 secreted into the culture supernatant was determined by Western blotting (*Upper*). The presence of the highly abundant surface antigen, SAG1, is shown as a control for equal parasite numbers. The amount of MIC2 secreted relative to vehicle-treated controls was measured by densitometry (*Lower*). Data are mean values ± SEMs of three independent experiments and are expressed as percentages of solvent-treated (DMSO) controls. EC_{50} values were calculated according to the average percentage inhibition of MIC2 secretion relative to DMSO-treated controls.

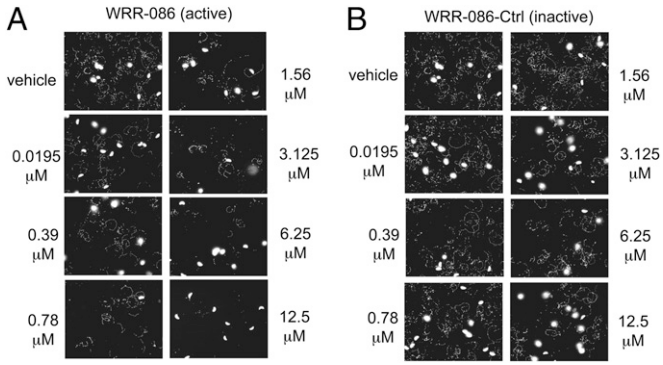

Fig. S6. WRR-086 inhibits parasite motility. Dose–response of WRR-086 (*A*) and WRR-086-Ctrl (*B*) in gliding motility. Parasites were pretreated with vehicle or varying concentrations of WRR-086 and WRR-086-Ctrl. Trails deposited by parasites were visualized by indirect immunofluorescence microscopy using an antibody that recognizes the highly abundant surface protein, SAG1. Representative images are shown.

Table S1. List of all of the identified proteins from on-bead digestion of probe-labeled proteins

ToxoDB GeneID	Description	Avg. spectral counts probe only	SE	Avg. spectral counts WRR-086 pretreated	SE	Fold change
TGME49_033140	Deoxyuridine 5′-triphosphate nucleotidohydrolase, putative	24.17	9.45	6.33	0.88	3.82
TGME49_053290	Valyl-tRNA synthetase, putative	74.00	4.26	23.17	3.83	3.19
TGME49_040980	Hypothetical protein	17.00	1.63	5.33	1.82	3.19
TGME49_121420	Kelch motif domain-containing protein	14.50	1.15	4.83	0.91	3.00
TGME49_088460	Hypothetical protein	12.50	1.59	4.67	1.28	2.68
TGME49_089690	Glyceraldehyde-3-phosphate dehydrogenase	256.50	80.90	101.67	20.71	2.52
TGME49_030990	Hypothetical protein	10.83	1.58	4.83	1.14	2.24
TGME49_118430	Malate dehydrogenase, putative	9.33	0.71	4.17	1.49	2.24
TGME49_111890	Hypothetical protein	12.17	1.66	5.50	1.82	2.21
TGME49_110640	Uridine phosphorylase, putative	244.67	38.12	114.17	13.13	2.14
TGME49_105800	Hypothetical protein, conserved	14.67	1.26	7.33	1.82	2.00
TGME49_066990	Coatomer β subunit, putative/β-coat protein, putative	14.17	2.44	7.17	1.72	1.98
TGME49_077760	Hypothetical protein, conserved	10.00	1.46	5.17	1.45	1.94
TGME49_073460	Eukaryotic translation initiation factor 3 subunit 6 interacting protein, putative	26.33	5.52	13.67	3.49	1.93
TGME49_035620	Deoxyhypusine synthase, putative	21.33	1.36	11.17	1.25	1.91
TGME49_043730	p36 protein	8.83	1.30	4.67	1.63	1.89
TGME49_080490	Ubiquitin conjugation factor-related	20.17	1.11	10.67	2.39	1.89
TGME49_003750	Hypothetical protein	7.67	0.42	4.17	1.35	1.84
TGME49_021470	Hypothetical protein	15.17	3.27	8.67	2.19	1.75
TGME49_073370	Coatomer protein gamma 2-subunit, putative	7.00	1.10	4.00	1.48	1.75
TGME49_090670	Cytosol aminopeptidase	338.33	30.46	195.00	17.63	1.74
TGME49_032660	58-kDa phosphoprotein, putative	14.33	4.06	8.33	1.78	1.72
TGME49_014290	Intracellular protease, putative	131.67	25.66	77.33	12.24	1.70
TGME49_113410	26S proteasome non-ATPase regulatory subunit 2, putative	15.17	1.30	9.00	2.14	1.69
TGME49_016900	Hypothetical protein	16.83	3.81	10.00	3.70	1.68
TGME49_070550	γ-glutamyl phosphate reductase, putative	9.50	1.18	5.67	1.28	1.68
TGME49_005130	Glyoxalase, putative	8.33	1.36	5.00	1.34	1.67
TGME49_042070	cAMP-dependent protein kinase regulatory subunit, putative	26.17	5.17	16.17	1.76	1.62
TGME49_026960	Phosphofructokinase, putative	484.50	68.95	300.33	30.62	1.61
TGME49_106960	Phenylalanyl-tRNA synthetase β chain, putative	16.67	1.28	10.33	2.08	1.61
TGME49_094620	Eukaryotic translation initiation factor 3 subunit 8, putative	9.33	0.88	5.83	1.35	1.60
TGME49_083560	Hypothetical protein	7.17	1.19	4.50	1.71	1.59
TGME49_029000	Kelch motif domain-containing protein	32.67	4.75	20.67	2.11	1.58
TGME49_022430	Ubiquitin-transferase domain containing protein	11.83	2.10	7.50	1.56	1.58
TGME49_015040	Hypothetical protein	12.33	2.62	8.00	3.32	1.54
TGME49_019710	Hypothetical protein	23.33	6.44	15.17	4.76	1.54
TGME49_026730	Aconitate hydratase, putative	31.50	11.29	20.50	6.43	1.54
TGME49_074190	Eukaryotic initiation factor 2B epsilon subunit, putative	9.83	1.60	6.50	1.56	1.51
TGME49_090200	Opine dehydrogenase, putative	7.67	0.95	5.17	1.33	1.48
TGME49_030960	Splicing factor 3B subunit 3, putative	6.17	1.08	4.17	1.56	1.48
TGME49_039620	Nucleotidase, putative	15.67	1.56	10.67	0.84	1.47
TGME49_056970	Vacuolar ATP synthase catalytic subunit A, putative	8.50	1.15	5.83	1.38	1.46
TGME49_023020	Coproporphyrinogen oxidase, putative	8.00	0.86	5.50	1.34	1.45
TGME49_089190	TPR domain-containing protein	7.00	1.15	4.83	1.28	1.45
TGME49_109210	Peroxidoxin 2	20.33	6.14	14.17	3.46	1.44
TGME49_091680	Protein transport protein Sec23, putative	9.00	1.57	6.33	1.71	1.42

Table S1. Cont.

ToxoDB GeneID	Description	Avg. spectral counts probe only	SE	Avg. spectral counts WRR-086 pretreated	SE	Fold change
TGME49_059880	Hypothetical protein	13.17	2.55	9.33	3.19	1.41
TGME49_109370	Adaptin, putative	6.33	0.49	4.50	0.96	1.41
TGME49_089650	Phosphoenolpyruvate carboxykinase, putative	214.00	20.77	153.33	22.45	1.40
TGME49_020400	Actin depolymerizing factor	11.83	1.14	8.50	2.00	1.39
TGME49_009960	Glycan synthetase, putative	6.00	0.77	4.33	1.14	1.38
TGME49_094350	DEAD/DEAH box helicase, putative	8.00	1.03	5.83	1.25	1.37
TGME49_029180	Importin β-3 subunit, putative	43.17	4.72	31.67	1.63	1.36
TGME49_075650	p97 protein	16.50	3.55	12.17	2.95	1.36
TGME49_121620	Dynamin-like protein, putative	19.00	1.84	14.17	3.37	1.34
TGME49_080560	Selenophosphate synthetase, putative	11.33	1.87	8.50	1.98	1.33
TGME49_031480	Translational activator, putative	16.00	2.44	12.00	2.86	1.33
TGME49_067050	Hypothetical protein	6.00	0.58	4.50	1.18	1.33
TGME49_028490	Hypothetical protein, conserved	8.00	1.37	6.00	1.59	1.33
TGME49_051690	Seryl-tRNA synthetase, putative	31.00	4.53	23.33	2.44	1.33
TGME49_053730	Importin-α re-exporter, putative	7.50	0.81	5.67	1.71	1.32
TGME49_089300	Methionyl-tRNA synthetase, putative	38.00	2.14	29.33	1.98	1.30
TGME49_035970	Eukaryotic translation initiation factor 2 gamma subunit, putative	9.50	1.94	7.33	0.95	1.30
TGME49_019520	Arginine *N*-methyltransferase 1	9.00	1.37	7.00	0.89	1.29
TGME49_097500	TCP-1/cpn60 family chaperonin, putative	14.00	0.86	11.33	1.14	1.24
TGME49_110030	Adenylyl cyclase associated protein	31.00	7.03	25.33	4.51	1.22
TGME49_049530	Exportin, putative	24.67	3.30	20.17	5.17	1.22
TGME49_085980	Phosphoglucomutase/parafusin related protein 1, putative	18.50	5.72	15.17	3.88	1.22
TGME49_001680	Eukaryotic translation initiation factor 3 subunit 10, putative	7.83	1.45	6.50	2.16	1.21
TGME49_094880	*N*-glycosylase/DNA lyase-related	11.17	0.70	9.33	2.26	1.20
TGME49_095040	Importin subunit β-1, putative	15.50	2.50	13.00	3.05	1.19
TGME49_090890	Carbonyl reductase, putative	9.50	2.01	8.00	1.21	1.19
TGME49_040890	Phosphofructokinase, putative	12.67	1.78	10.67	4.05	1.19
TGME49_039820	D-3-phosphoglycerate dehydrogenase, putative	43.33	2.94	36.83	2.43	1.18
TGME49_044690	Hypothetical protein	21.33	1.93	18.17	1.90	1.17
TGME49_100140	Elongation factor 1-gamma, putative	98.33	10.05	84.33	8.63	1.17
TGME49_064830	Hypothetical protein	19.00	2.18	16.33	2.50	1.16
TGME49_024890	Hypothetical protein, conserved	28.00	2.72	24.17	0.75	1.16
TGME49_093870	Thioredoxin, putative	62.00	10.24	53.67	7.25	1.16
TGME49_025060	Nucleoredoxin, putative	11.50	1.98	10.00	1.41	1.15
TGME49_015220	Hypothetical protein, conserved	10.00	2.44	8.83	2.52	1.13
TGME49_019850	Prolyl-tRNA synthetase, putative	26.33	4.66	23.33	1.80	1.13
TGME49_005560	Nascent polypeptide-associated complex α chain, putative	25.50	5.24	22.83	5.65	1.12
TGME49_091640	Aspartate carbamoyltransferase	18.00	2.25	16.17	1.64	1.11
TGME49_019310	Heat shock protein, putative	13.50	1.34	12.17	2.61	1.11
TGME49_110080	Long-chain-fatty-acid–CoA ligase, putative	15.33	4.00	13.83	4.57	1.11
TGME49_097060	Phosphoglycerate mutase 1, putative	19.33	2.86	17.50	1.91	1.10
TGME49_025050	Adenosylhomocysteinase, putative	12.67	2.44	11.50	2.72	1.10
TGME49_070510	Asparaginyl-tRNA synthetase, putative	36.50	2.79	33.33	2.55	1.10
TGME49_094200	Glucose-6-phosphate dehydrogenase	9.67	2.17	8.83	1.89	1.09
TGME49_026910	Glycogen debranching enzyme, putative	22.33	7.72	20.50	6.69	1.09
TGME49_071810	Inhibitor-1 of protein phosphatase type 2A	10.50	0.62	9.67	2.04	1.09
TGME49_031600	Importin, putative	23.17	1.47	21.33	1.73	1.09
TGME49_022380	Exportin 7, putative	13.83	2.24	12.83	3.26	1.08
TGME49_079380	Conserved Hypothetical protein	21.17	3.67	19.67	3.41	1.08
TGME49_087500	TCP-1/cpn60 family chaperonin, putative	10.00	1.37	9.33	1.12	1.07
TGME49_038070	PKC-interacting cousin of thioredoxin, putative	15.17	2.87	14.17	3.06	1.07
TGME49_078830	Glucose-6-phosphate dehydrogenase, putative	29.17	1.58	27.33	2.42	1.07
TGME49_099210	CTP synthase, putative	8.33	0.80	7.83	1.68	1.06
TGME49_066960	Tubulin β chain	17.17	4.17	16.17	6.61	1.06
TGME49_111400	Hypothetical protein, conserved	15.83	1.72	15.00	3.30	1.06

Table S1. Cont.

ToxoDB GeneID	Description	Avg. spectral counts probe only	SE	Avg. spectral counts WRR-086 pretreated	SE	Fold change
TGME49_001380	Chorismate synthase, putative	17.17	3.43	16.33	2.42	1.05
TGME49_047760	Long chain acyl-CoA synthetase, putative	14.17	1.45	13.50	2.75	1.05
TGME49_025930	Triosephosphate isomerase, putative	13.33	2.15	12.83	1.01	1.04
TGME49_016260	Eukaryotic initiation factor-2B gamma subunit, putative	13.67	1.71	13.17	0.48	1.04
TGME49_002530	Aspartyl-tRNA synthetase, putative	10.00	1.39	9.67	1.96	1.03
TGME49_016450	Proteasome subunit α type 3, putative	20.17	2.30	19.50	1.59	1.03
TGME49_043710	TCP-1/cpn60 family chaperonin, putative	37.50	1.98	36.33	3.67	1.03
TGME49_092080	Leucyl-tRNA synthetase, putative	16.83	2.56	16.33	3.52	1.03
TGME49_109730	Thioredoxin reductase, putative	114.17	11.66	111.17	11.45	1.03
TGME49_015260	Carbamoyl phosphate synthetase II	12.83	1.11	12.50	2.95	1.03
TGME49_090290	Ubiquitin-activating enzyme E1, putative	46.00	1.93	44.83	4.18	1.03
TGME49_057740	UMP-CMP kinase, putative	7.00	0.77	6.83	1.56	1.02
TGME49_065530	RNA binding motif-containing protein	8.67	1.05	8.50	3.02	1.02
TGME49_100260	Threonyl-tRNA synthetase, putative	17.50	1.02	17.17	1.72	1.02
TGME49_026250	ATP-dependent RNA helicase, putative	29.33	5.99	28.83	8.74	1.02
TGME49_010840	Arginyl-tRNA synthetase, putative	13.50	3.89	13.33	3.41	1.01
TGME49_089600	Hsp20/α crystallin domain-containing protein	21.17	4.14	21.00	4.86	1.01
TGME49_036570	Lysine decarboxylase domain-containing protein	6.50	0.99	6.50	1.38	1.00
TGME49_077000	Transport protein Sec24, putative	41.50	1.75	41.83	3.51	0.99
TGME49_017460	Tlutaminyl-tRNA synthetase, putative	13.67	1.69	13.83	2.95	0.99
TGME49_052290	Importin α, putative	13.33	1.58	13.50	1.20	0.99
TGME49_074070	thiF family domain-containing protein	12.00	1.21	12.17	0.60	0.99
TGME49_080380	Nontransmembrane antigen	11.33	1.36	11.50	0.76	0.99
TGME49_014350	GTP binding protein, putative	8.33	1.61	8.50	1.31	0.98
TGME49_043910	Haloacid dehalogenase-like hydrolase domain-containing protein	20.67	3.00	21.17	2.23	0.98
TGME49_009600	Hypothetical protein	32.17	10.51	33.00	9.34	0.97
TGME49_059550	Hydroxymethyldihydropterin pyrophosphokinase-dihydropteroate synthase	19.17	1.35	19.67	2.06	0.97
TGME49_019540	Alanyl-tRNA synthetase, putative	33.00	2.46	34.00	1.91	0.97
TGME49_072910	TCP-1/cpn60 family chaperonin, putative	10.00	1.83	10.33	1.20	0.97
TGME49_107850	6-phosphogluconate dehydrogenase, putative	6.67	0.67	7.00	1.71	0.95
TGME49_032350	Lactate dehydrogenase	146.50	19.76	153.83	13.60	0.95
TGME49_118230	Phosphoglycerate kinase, putative	33.00	3.14	34.67	2.50	0.95
TGME49_077240	Nucleoside-triphosphatase I	45.50	2.26	47.83	3.22	0.95
TGME49_030450	GMP synthase, putative	40.33	3.40	42.50	2.31	0.95
TGME49_016590	Transportin, putative	9.00	2.11	9.50	2.69	0.95
TGME49_032340	Protein phosphatase 2C, putative	8.00	0.58	8.50	2.04	0.94
TGME49_036040	Fructose-1,6-bisphosphate aldolase	44.00	5.43	47.00	8.73	0.94
TGME49_112630	Hypothetical protein	62.83	5.18	67.33	7.95	0.93
TGME49_009030	Actin	108.33	5.98	116.33	13.64	0.93
TGME49_016860	ATP-dependent RNA helicase, putative	13.50	2.09	14.50	2.04	0.93
TGME49_049180	Bifunctional dihydrofolate reductase-thymidylate synthase (DHFR-TS)	51.67	4.36	55.67	3.90	0.93
TGME49_093180	NADP-specific glutamate dehydrogenase, putative	30.67	1.82	33.17	2.80	0.92
TGME49_013870	Ubiquitin carboxyl-terminal hydrolase, putative	16.83	1.81	18.33	1.58	0.92
TGME49_011680	Protein disulfide isomerase, putative	76.17	12.40	83.00	11.55	0.92
TGME49_016880	Receptor for activated C kinase, RACK protein, putative	9.17	1.56	10.00	2.13	0.92
TGME49_080600	Histidyl-tRNA synthetase, putative	37.50	4.39	41.00	2.00	0.91
TGME49_068950	la domain-containing protein	17.83	2.10	19.50	4.07	0.91
TGME49_089330	Ubiquitin carboxyl-terminal hydrolase, putative	31.83	3.65	34.83	4.34	0.91
TGME49_047510	Fructose-1,6-bisphosphatase, putative	7.00	0.52	7.67	1.61	0.91
TGME49_077270	Nucleoside-triphosphatase II	39.83	1.85	43.67	3.67	0.91
TGME49_002370	TCP-1/cpn60 family chaperonin, putative	8.50	2.01	9.33	1.43	0.91
TGME49_073090	VIcell division protein 48, putative	23.33	1.26	25.67	3.37	0.91
TGME49_022160	Aldehyde dehydrogenase, putative	9.50	1.87	10.50	1.31	0.90
TGME49_053430	Asparagine synthase, putative	36.00	4.57	39.83	2.60	0.90

Table S1. Cont.

ToxoDB GeneID	Description	Avg. spectral counts probe only	SE	Avg. spectral counts WRR-086 pretreated	SE	Fold change
TGME49_005440	TCP-1/cpn60 family chaperonin, putative	7.33	1.73	8.17	0.54	0.90
TGME49_050770	Eukaryotic translation initiation factor 4A	31.50	1.87	35.33	3.05	0.89
TGME49_033110	Inosine-5′-monophosphate dehydrogenase, putative	9.33	2.22	10.50	0.56	0.89
TGME49_065450	Hexokinase	53.33	4.69	60.17	7.72	0.89
TGME49_032300	40S ribosomal protein S3, putative	7.17	1.30	8.17	0.83	0.88
TGME49_002380	rab GDP dissociation inhibitor α, putative	8.33	1.74	9.50	1.23	0.88
TGME49_088380	Heat shock protein 90	57.83	3.67	66.00	4.91	0.88
TGME49_020860	DEAD/DEAH box helicase, putative	6.67	0.80	7.67	1.36	0.87
TGME49_107570	Glycerol-3-phosphate dehydrogenase, putative	7.67	0.88	8.83	1.28	0.87
TGME49_049390	NAD-specific glutamate dehydrogenase, putative	34.33	2.70	39.67	5.17	0.87
TGME49_031850	Serine-threonine phosophatase 2C	17.67	1.43	20.50	1.43	0.86
TGME49_086750	MA3 domain protein	8.17	1.11	9.50	0.72	0.86
TGME49_097720	Trehalose-6-phosphate synthase domain-containing protein	7.00	0.58	8.17	2.33	0.86
TGME49_065330	CMGC kinase, GSK family TgPK3	10.50	2.32	12.33	1.05	0.85
TGME49_056990	Glycyl-tRNA synthetase, putative	26.50	2.95	31.17	3.08	0.85
TGME49_007640	Isoleucine-tRNA synthetase, putative	7.17	0.70	8.50	2.06	0.84
TGME49_038050	Tudor/staphylococcal nuclease domain-containing protein	19.00	3.49	22.67	4.63	0.84
TGME49_061600	X-prolyl aminopeptidase, putative	9.50	1.45	11.33	3.07	0.84
TGME49_068850	Enolase, putative	257.83	28.20	309.50	38.05	0.83
TGME49_005700	20k cyclophilin precursor	15.83	1.66	19.17	1.68	0.83
TGME49_088360	Tryptophanyl-tRNA synthetase, putative	31.00	3.91	38.33	1.71	0.81
TGME49_083780	Glucose-6-phosphate isomerase, putative	15.50	1.73	19.17	3.07	0.81
TGME49_014490	M16 family peptidase, putative	16.50	2.51	20.50	2.31	0.80
TGME49_088630	Nucleosome assembly domain-containing protein	38.50	5.90	48.00	5.03	0.80
TGME49_093690	Profilin family protein	18.00	2.98	22.50	4.50	0.80
TGME49_086420	Elongation factor 1-α, putative	226.50	29.45	285.67	36.33	0.79
TGME49_094800	Elongation factor 1-α, putative	226.50	29.45	285.67	36.33	0.79
TGME49_023070	Hypothetical protein	12.00	1.15	15.33	1.65	0.78
TGME49_110670	Glycogen phosphorylase, putative	9.50	0.88	12.17	3.03	0.78
TGME49_005470	Elongation factor 2, putative	148.83	3.76	191.00	25.09	0.78
TGME49_073760	Heat shock protein 70, putative	64.17	3.92	82.50	6.59	0.78
TGME49_048340	GTP-binding nuclear protein RAN/TC4, putative	15.17	0.95	19.50	1.82	0.78
TGME49_014260	α-glucan water dikinase 1, putative	5.50	1.02	7.50	2.16	0.73
TGME49_118580	Phosphoglucomutase, putative	9.00	1.03	12.33	0.99	0.73
TGME49_046330	CRAL/TRIO domain-containing protein	6.67	1.20	9.17	1.92	0.73
TGME49_032250	Peroxisomal catalase	21.00	4.67	29.00	5.46	0.72
TGME49_056760	Pyruvate kinase, putative	33.50	1.09	46.67	4.85	0.72
TGME49_093370	Arginine *N*-methyltransferase-related	5.00	0.86	7.00	2.41	0.71
TGME49_016650	Hypothetical protein, conserved	18.67	3.90	26.17	4.22	0.71
TGME49_063090	14-3-3 protein, putative	21.50	1.87	30.33	2.68	0.71
TGME49_063870	Glutamyl-tRNA synthetase, putative	8.00	1.26	11.50	2.35	0.70
TGME49_017890	Peroxiredoxin	33.83	7.40	48.67	6.38	0.70
TGME49_049780	Hypothetical protein	10.83	1.56	15.67	2.27	0.69
TGME49_108920	U2 small nuclear ribonucleoprotein auxiliary factor (U2AF) 2	6.33	1.12	9.33	2.04	0.68
TGME49_078050	Proteasome subunit α type 1, putative	8.50	1.52	12.67	1.80	0.67
TGME49_083850	Peptidyl-prolyl isomerase, putative	35.50	3.66	54.17	9.00	0.66
TGME49_101440	CAM kinase, CDPK family TgCDPK1	17.33	1.05	27.17	1.14	0.64
TGME49_026410	Elongation factor 1-β, putative	20.50	1.84	32.17	4.82	0.64
TGME49_062100	TPR domain-containing protein	5.00	0.93	8.67	1.36	0.58
TGME49_032440	Hypothetical protein	3.67	0.88	6.50	1.67	0.56
TGME49_115270	Hypothetical protein	5.17	1.08	10.50	1.94	0.49
TGME49_066640	Acetyl-CoA synthetase, putative	41.17	5.39	85.33	3.86	0.48

Table S2. List of proteins identified as having specific modification of a cysteine residue by WRR-086

ToxoDB Gene ID	Protein	Modified peptide	Total spectral counts	Xcorr	DeltaCN
TGME49_110640	Uridine phosphorylase, putative	K.KGDLASLIVTVGC*EQR.A	361	4.744	0.239
TGME49_005470	Elognation factor 2, putative	R.VTDGALVVVDTIEGVC*VQTETVLR.Q	65	5.4313	0.427
TGME49_068850	Enolase, putative	R.GNPTVEVDLLTDGGC*FR.A	47	3.0161	0.2673
TGME49_014290	Intracellular protease, putative	K.AVAYPC*FMDQFPADMR.G	26	3.2806	0.0779
TGME49_063530	10-kDa heat shock protein, mitochondrial, putative	K.TGEFIPPC*VQVGQTVVPEYGGMK.V	25	4.3777	0.2986
TGME49_089690	Cytosol aminopeptidase	K.TVAVVLPTC*QK.V	20	3.6775	0.2795
TGME49_040600	TCP-1/cpn60 family chaperone, putative	K.AEMTC*DGDDPVGAAAEVVDEMEGEIELQK.A	12	7.6504	0.4735
TGME49_029000	Kelch motif domain-containing protein	R.LAPVC*TTFSVLDVR.R	8	2.813	0.1797
TGME49_080740	Signal peptidase, putative	R.AVMPAC*IQQLFQAVGDELR.S	8	5.336	0.102
TGME49_049180	Bifunctional dihydrofolate reductase-thymidylate synthase (DHFR-TS)	K.STAAQAAAPAESVFVPFC*PELGR.E	7	5.3617	0.3183
TGME49_090670	Glyceraldehyde-3-phosphate dehydrogenase	K.GIISYTDEEVVSSDFVHC*K.F	6	3.5372	0.4026
TGME49_070120	Thioredoxin, putative	K.VVQFSASWC*GPCR.Q	5	2.5886	0.2017
TGME49_002890	Hypothetical protein	R.IGPAYQAPIPDC*IR.D	4	3.0733	0.2152
TGME49_026250	ATP-dependent RNA helicase, putative	K.QDIPSFLPPLVLSC*TSSSSR.M	4	3.4077	0.1323
TGME49_029930	p25-α domain-containing protein	R.GQAAGLGPSGATAQISLADIC*DR.S	4	5.7366	0.3678
TGME49_088500	Malate:quinone oxidoreductase, putative	R.RPSFAVVASC*PR.N	4	2.8942	0.0898
TGME49_090890	Carbonyl reductase, putative	R.IISVASMC*GK.M	4	2.6978	0.244
TGME49_093180	NADP-specific glutamate dehydrogenase, putative	K.NLSVVTPPELVTDDPGDMPDC*K.I	4	4.0162	0.1232
TGME49_040980	Hypothetical protein	R.EQSEEPIEFPAC*LAISALAIK.A	3	3.5842	0.1817
TGME49_047550	Heat shock protein 60	R.IQDALC*ATK.A	3	2.6219	0.1391
TGME49_047600	Conserved hypothetical protein	R.AVTALLDLQNFGSC*ASTAGEELVK.T	3	4.1774	0.3276
TGME49_009190	ABC transporter, putative	R.TLLYMPPSLFLC*R.S	2	2.2334	0.1221
TGME49_011680	Protein disulfide isomerase, putative	K.DKDVMLEIYAPWC*GYCK.S	2	3.5398	0.1309
TGME49_032250	Peroxisomal catalase	R.AIGLPTAAC*YPAK.M	2	2.6228	0.1308
TGME49_032350	Lactate dehydrogenase	K.TFIIVVTNPLDC*MVK.V	2	2.5998	0.1515
GME49_029180	Importin β-3 subunit, putative	K.VAMEAMLQIAESTATC*EDTK.T	2	4.0493	0.2022
TGME49_032370	CW-type zinc finger domain-containing protein	K.GAPAVC*VAGASPPAAK.K	2	3.7818	0.2255
TGME49_043460	Hypothetical protein	R.LSTGGVISSFESSAEGIC*AALSLR.R	2	4.8717	0.3967
TGME49_040980	Hypothetical protein	R.SSFQQLAC*TR.Q	2	2.6021	0.1328
TGME49_049910	Mitochondria-associated granulocyte macrophage CSF signaling molecule, putative	R.ILGLDSSGSSSAPLC*R.Q	2	3.2511	0.1881
TGME49_070120	Thioredoxin, putative	K.VTDSEEDC*SVK.V	2	3.651	0.1147
TGME49_118600	DNA/panthothenate metabolism flavoprotein domain-containing protein	R.TDGGNVVLGEGC*IEAQLVQVVNQLR.T	2	4.5677	0.253
TGME49_086260	Hypothetical protein	R.ALGFYLEQLLQDDLLC*K.E	2	3.6584	0.1852

Table S3. Parasites were treated with vehicle (DMSO) for 15 min at 25 °C before performing the Endo-synchronized attachment/invasion assay

Variable	Attachment (DMSO; no. of parasites per field)	Invaded (DMSO; % invaded cells per field)
RHdelta	40.7	85.2
DJ1WT	41.1	90.1
C127A	35.5	85.6
C127S	42.7	87.4

Attachment data represent the average of three independent experiments and were calculated as the average total number of parasites (extracellular and intracellular) per field from 10 randomly selected fields. Invasion data represent the average percentage of invaded parasites from 10 randomly selected fields from three independent experiments.